

# ELECTRON MICROSCOPY IN THE CATALYSIS OF ALKANE OXIDATION, ENVIRONMENTAL CONTROL, AND ALTERNATIVE ENERGY SOURCES

---

Pratibha L. Gai

*DuPont, Central Research and Development Laboratories, Experimental Station, Wilmington, Delaware 19880-0356, and Department of Materials Science and Engineering, University of Delaware, Newark, Delaware 19716;*  
email: pratibha.l.gai@usa.dupont.com

Jose J. Calvino

*Departamento de Ciencia de los Materiales e Ing. Met. y Química Inorgánica, Facultad de Ciencias de la Universidad de Cádiz, Spain; email: jose.calvino@uca.es*

**Key Words** hydrocarbon technology, environmental catalysts, in situ ETEM, TEM, nanostructures, hydrogen energy

■ **Abstract** The key role of electron microscopy in understanding and creating advanced catalyst materials and processes in selective alkane oxidation, environmental control, and alternative energy sources is reviewed. In many technological processes, catalysts are increasingly nanoscale heterogeneous materials. With growing regulatory guidelines requiring efficient and environmentally compatible catalytic processes, it is crucial to have a fundamental understanding of the catalyst nanostructure and modes of operation under reaction conditions to design novel catalysts and processes. The review highlights the pioneering development and applications of atomic resolution in situ-environmental transmission electron microscopy (ETEM) for probing dynamic catalysis directly at the atomic level, high-resolution electron microscopy, and analytical spectroscopic methods in the development of alkane catalyzation, environmental protection, and new energy sources.

## INTRODUCTION

The selective oxidation of hydrocarbons to a variety of industrial polymer products and novel routes for environmental catalysis have received considerable interest (1). The selective oxidation of n-butane to maleic anhydride (MA) is an important commercial process. Maleic anhydride is used as a raw material for a variety of products ranging from tetrahydrofurans (THF) for industrial fibers and polyurethane technologies to agricultural chemicals. Several international groups are working to improve the process. The oxidation of n-butane to MA is a remarkably selective 14-electron oxidation. To date, vanadium phosphorus oxide-based catalysts are still

the most active and selective systems for this chemistry. It is likely, however, that other highly active and selective catalysts exist, with possibly different properties (stability and lattice oxygen capacity). However, to date, none has been discovered. Significant progress in the area is being made by studying catalysts under in situ conditions. By understanding the nature of active species, more stable and active catalysts (e.g., those having higher surface areas, or placed on high surface area supports) could be developed.

Also, environmental concern is undoubtedly a powerful driving force, particularly in catalysis. Thus the topic of environmental catalysis has established itself as an area of increasing interest that encompasses a variety of technical approaches, all of which have the common goal of improving the quality of the natural environment and contributing to so-called sustainable development (2). Generally speaking, environmental catalysis is not only related to technologies aimed at correcting or controlling emissions to the environment of noxious pollutant substances but also to areas such as green chemistry or alternative energy sources. The search for catalytic processes that allow higher selectivity (i.e., less undesired by-products); lower energy consumptions; diversification of fuels; improvements in the quality of fuels; or for alternative, more environmentally benign energy sources are also the scope of this exciting, ever-growing field. In this review we highlight the key role of electron microscopy (EM) methods in recent advances in promoted catalysts for butane oxidation as well as environmental and energy catalysis.

## EXPERIMENTAL PROCEDURES

### Electron Microscopy Techniques

Electron microscopy techniques are powerful and versatile research tools for investigating the local structure and chemistry of complex heterogeneous catalysts directly, from the macroscopic to the atomic scale (3, 4). Several monographic books, issues and articles on EM of catalysis clearly demonstrate the tremendous impact of these techniques in the characterization of catalytic solids (5–17).

Briefly, EM provides structural information of samples in both the real space and reciprocal space. It provides local structural information of the surface and the bulk of the sample routinely at the atomic level and also provides chemical, electronic, and three-dimensional structural information. EM is a diffraction technique in which crystals diffract electrons in accordance with Bragg's Law,  $n\lambda = 2d_{hkl}\sin\theta$ , where  $\lambda$  is the wavelength of electrons,  $d$  is the lattice planar spacing of  $hkl$  reflection, and  $\theta$  is the scattering angle. The diffraction pattern thus formed may be regarded as a Fourier transform (FT) of the crystal. An apertured inverse FT in the objective lens of the EM forms the image. The interactions of electrons with matter generates elastic scattering and a variety of other signals that can be used to obtain the structural and chemical information of a sample. Elastic scattering occurs when incident electrons interact with the potential field of nuclei of matter

with no energy loss in momentum transfer, whereas inelastic scattering occurs when interactions between incident electrons with electrons of matter occur and scattered electrons lose energy (3).

In a conventional transmission electron microscope (TEM) and high-resolution TEM (HRTEM), electrons transmit through the sample. The TEM has an electron gun and electromagnetic lenses, which include condenser and objective lenses, and operates at ambient temperature in high vacuum. TEM diffraction contrast is the conventional TEM imaging technique where the Bragg condition is satisfied for a single diffracted beam (3). If only the diffracted beam corresponding to the incident electron beam direction (primary beam containing the direct transmitted electrons) is used for imaging, a bright-field (bf) image is obtained; if only scattered electrons are used, a dark-field (df) image is formed. Defects such as point and extended defects control properties of catalysts, and understanding them is critical for controlling and optimizing catalytic properties. The diffraction contrast technique is particularly effective for determining the nature of defects (i.e., lattice imperfections), generally without detailed simulations of defect models. One of the most powerful methods of direct structural analysis of catalysts is HRTEM, where two or more Bragg reflections are used for imaging. The power of HRTEM in determining real-space structures of complex inorganic solids that were beyond the reach of conventional structural techniques (e.g., X-ray, neutron crystallography) has been elucidated by several workers (1, 5). Unlike conventional diffraction techniques [powder X-ray diffraction (XRD), neutron], HRTEM provides localized real-space information, now routinely at the atomic level, about the bulk and surface properties of solids, the corresponding chemical information, as well as electron diffraction information in reciprocal space.

For EM of catalysts, as-synthesized powders may be used. They are dispersed in alcohol and deposited on generally 3-mm-carbon-film beryllium, copper, or aluminum grids. If carbon or other support films are not desirable, finely meshed metal grids can be used. High purity grids should be used for experiments. The powders are thin enough for the electron beam to penetrate, and no further sample preparations are usually necessary.

Chemical composition analysis in the EM is carried out using electron-stimulated energy dispersive X-ray spectroscopy (EDX or EDS) or electron energy-loss spectroscopy (EELS). In EDX, X-rays with energies characteristic of elements are measured in the probed region of the sample. In EELS, energy losses produced by the interaction between incident electrons and the sample are measured. The energy losses result from inelastic scattering effects. EELS has normally been used to detect light elements in materials. The measurements via EELS spectra can provide quantitative information about chemical or oxidation states and elemental or chemical compositions and can be particularly effective in catalyst studies. Rich spectroscopic and structural information can be retrieved at atomic scale resolution, and with high energy resolution in the case of spectroscopic signals, which allows us to scrutinize the bulk, surface, and interface details of all types of materials. Thus TEM provides a set of highly complementary tools that allow

a very precise examination of materials in general (3) and of catalytic materials in particular (5–17).

## Recent Advances in Atomic Resolution In Situ ETEM for Probing Catalysis Directly at the Atomic Level

Heterogeneous catalysis is a dynamic process. In gas-catalyst reactions, the dynamic atomic structure of catalysts under operating conditions plays a pivotal role in governing catalytic properties. Therefore, there is a strong need for in situ EM methods for direct probing of live catalyst-gas molecule reactions, reaction mechanisms, transient species, and the chemistry of catalysts under reaction conditions. Furthermore, post-reaction examination of a static catalyst, which is taken out of the reaction environment and cooled to room temperature (RT), does not often represent the dynamic state of the catalyst and there may well be atmospheric contamination, which can cause errors in interpretation.

In ETEM, a gas reaction cell (or environmental cell, ECELL or microreactor) is integrated inside an electron microscope column, which is differentially pumped as described by Gai (7). Recent developments include atomic resolution in situ ETEM (also referred to as environmental-HRTEM), pioneered by Gai & Boyes (18, 19). It enables probing of dynamic chemical reaction processes directly at the atomic level. In this development, a new approach has been taken to design the ETEM, with radial holes in the objective lens pole pieces for gas feed, and the ECELL is integral to the ETEM (Figure 1a). The ETEM design of Gai & Boyes has been adopted by commercial TEM manufacturers (FEI) and copied globally.

In in situ ETEM studies, appropriate gas compositions, using a conventional reactor-type gas-manifold system, enable the inlet of flowing gases into the ETEM microreactor. A mass spectrometer is added for gas analysis. A sample stage with a furnace allows samples to be heated in the in situ ETEM (20–22) (Figure 1b). Lower gas pressures (a few mbar) are used for high-resolution imaging. Higher gas pressures are possible with some loss of resolution owing to multiple scattering of electrons through gas layers. Experiments on a large number of catalysts (5) have shown that the gas layer in immediate contact with the catalyst surface is the most critical to the catalytic reaction as compared with the total amount of gas present. Careful experimental conditions are used in in situ ETEM to ensure that the material is not damaged in the electron beam (12, 19, 20, 22a,b). These include the use of very-low-dose electron beam currents for imaging materials. The image signal is then amplified by a low-light television camera connected to a video monitor, or recorded on a charge-coupled device (CCD) camera. Calibration blank experiments (without the electron beam) are carried out with the beam switched on for a few seconds only to record the final state of the materials and to check with in situ data. Under these careful conditions, no invasive beam damage is observed. The pioneering atomic resolution ETEM development of Gai & Boyes has been highlighted by the American Chemical Society's *C&ENews* (23, 24). Parallel chemical

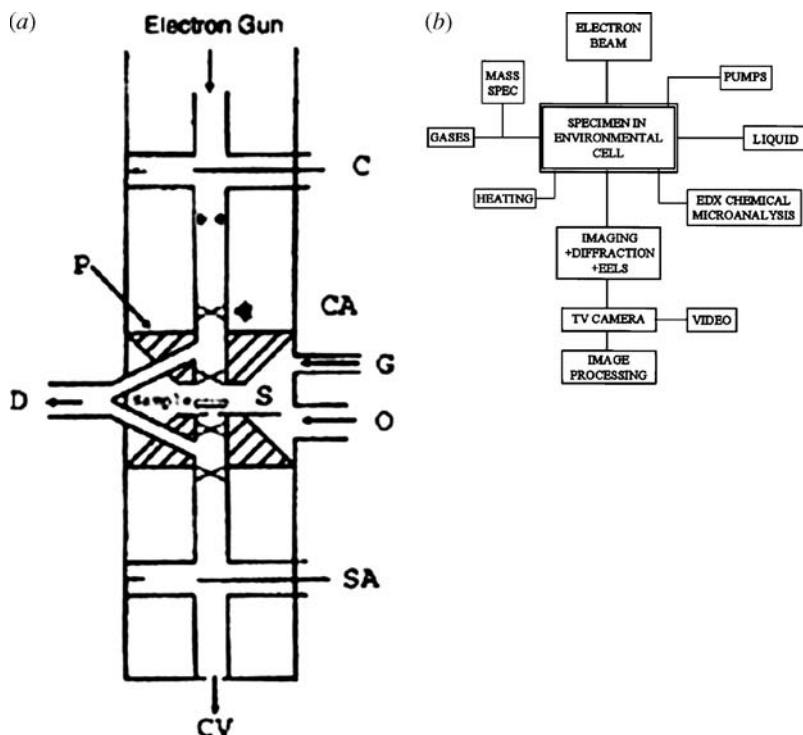


**Figure 1** (a) Schematic of atomic resolution in situ environmental transmission electron microscope (ETEM) with environmental cell (ECELL or microreactor), showing radial holes through objective lens pole pieces for gas lines (D). Differential pumping is used. P, pole pieces; CA, cell aperture; O, objective aperture; SA, selected area aperture; S, sample; G, gas; C, condenser aperture (18, 19). (b) Schematic of various components of ETEM.

reaction experiments have been performed on larger amounts ( $\sim 1$  g) of the sample in a microreactor to correlate microstructural observations with catalytic reactivity properties. Complementary techniques in catalytic chemistry involve temperature programmed (TP), oxidation state, and BET (Brunauer-Emmett-Teller) surface area measurements and powder XRD of samples.

Recent in situ developments also include of wet-environmental transmission electron microscopy (hereafter referred to as Wet-ETEM) to directly probe controlled liquid-catalyst reactions in liquid phase hydrogenation and polymerization at operating temperatures, at the nanomolecular scale (25, 26). This method opens up new opportunities for high-resolution studies of a wide range of solution-solid and solution-gas-solid reactions in the chemical, polymer, and biological sciences. Other EM methods generally used in catalysis are scanning electron microscopy (SEM) and scanning TEM (STEM) (27). SEM utilizes a focused electron beam

that systematically scans across the surface of a sample and is used to characterize surface topography of bulk powders or pellets (28, 29). STEM, which is essentially a combination of scanning EM and TEM, is powerful as a structural and an analytical tool and uses a finely focused probe ( $<1$  nm) over a thin sample (30). An important method in high resolution STEM is high angle annular dark field (HAADF) for Z (or atomic number)-contrast imaging (27). It utilizes the fact that high-angle scattering (angles  $>30$  mrad) obeys the Rutherford law, i.e., the scattering cross section is proportional to  $Z^2$ . The use of HAADF-STEM signal removes the complexity of conventional bright field scattering and the associated diffraction complications. The use of HAADF-STEM to determine the three-dimensional structure of supported metal nanocatalysts at a very high spatial resolution of  $<1$  nm has been demonstrated recently for Pd-Ru nanocatalysts supported on mesoporous silica (31).

## CATALYST SYNTHESIS AND IN SITU CHARACTERIZATION IN N-BUTANE CATALYSIS

### Control (Base) Catalysts

The most successful industrial process to manufacture MA is the vapor phase oxidation of n-butane over active vanadyl pyrophosphate catalysts (32). In the following, we review highlights of the recent work and the crucial role of EM, especially atomic resolution in situ ETEM, dynamic electron diffraction, and correlations of the catalyst microstructure with its reactivity. We review the effect of steam and cation promoters on catalyst performance. In the selective oxidation of the alkane to MA, the most active and selective phase is believed to be vanadyl pyrophosphate  $[(VO)_2P_2O_7]$  catalysts (hereafter referred to as VPO), with active centers located at the exposed (010) basal planes (20, 32). There are also some claims that the active phase is a combination of VPO and  $VOPO_4$  phases, or a P-rich phase, or a mixture of VPO with unknown or amorphous phases (32, 33). VPO is orthorhombic with  $a = 1.659$  nm,  $b = 0.776$  nm, and  $c = 0.9588$  nm (32, 34). VPO is a layered structure and the basal (010) plane, considered to be the active plane, consists of edge-sharing pairs of distorted vanadium octahedra shared at corners by the phosphate tetrahedral groups (Figure 2a). An organic method is generally employed to synthesize the base catalyst precursors (20, 32, 35, 36). Vanadium pentoxide and anhydrous phosphoric acid, prepared by mixing  $P_2O_5$  with aqueous phosphoric acid, are refluxed in 11:1 isobutyl alcohol/benzyl alcohol solvent mixtures under an inert atmosphere. Enough anhydrous phosphoric acid to satisfy a 1.1/1, P/V atomic ratio is slowly added to the alcohol mixture over a period of a couple of hours. The solution is allowed to reflux for several hours. Soluble pentavalent vanadyl species are reduced predominantly by benzyl alcohol to precipitate the blue tetravalent precursor (which is the case of pure VPO catalysts), which crystallizes as vanadium hydrogen phosphate hemihydrate,  $VO(HPO_4) \cdot 0.5 H_2O$ . The precursors are subsequently dried in vacuum at  $150^\circ C$  for 18 h.

Bartley (37) described vanadium (V) phosphate prepared using a solvent-free (in the absence of water) leading to an anhydrous  $\text{VOPO}_4$  that can be readily hydrated to the precursor.

## Promoted Catalysts

In the case of promoted VPO catalysts, promoter cations are added as the soluble chlorides and alkoxides, which subsequently coprecipitate. A number of single metal cations (e.g., Fe, Cr, Ce, Li, Zn) have been added (38–41), and the literature connected to the promotion of VPO catalysts has been reviewed recently by Hutchings and coworkers (40). ETEM, SEM, and diffraction methods play a key role in elucidating the surface and bulk microstructural changes, which are due to the catalyst promotion, and the interplay between the promoted structures and reactivity to obtain a deeper understanding of the role of promoted microstructures in the alkane oxidation catalysis.

Gai and coworkers (35, 36) have synthesized promoted catalysts with cations of two metals substituting for V. Their approach has been to replace  $\text{V}^{4+}$  with an equimolar combination of cations of different valencies such as  $\text{Fe}^{3+}$  and  $\text{Sb}^{5+}$  or bismuth and molybdenum (36). They have compared catalyst performance from this approach with that involving the substitution of a lower valent cation such as  $\text{Fe}^{3+}$  or  $\text{Cr}^{3+}$  for  $\text{V}^{4+}$ , as well as cerium oxide additions as an oxygen reservoir to the VPO catalyst. In addition they have prepared novel, grafted-promoted VPO catalysts as alternative synthetic pathways.

To create the novel grafted-promoted vanadium phosphate catalyst, a mixture of bismuth and molybdenum alkoxides is used with the hemihydrate precursor. The alkoxides, prepared using bismuth and molybdenum chloride, form a soluble, mixed alkoxide complex when reacted with ethanol. The mixed alkoxide, dissolved in alcohol, is reactively grafted onto the preformed precursor. The catalysts in these experiments contain only 1 mol% bismuth and molybdenum supported on  $\text{VOHPO}_4 \cdot \frac{1}{2}\text{H}_2\text{O}$ . This process is a grafting procedure, and the precursor complex is then heated to transform into the final, promoted catalyst. Calcinations are performed in a small, 3.5-cm fluidized bed on 60 g catalyst samples. Samples are heated in air at  $390^\circ\text{C}$  for 1 h, followed by  $460^\circ\text{C}$  for 18 h in 1.5% butane/air. The relatively high temperature of  $460^\circ\text{C}$  used for the calcination is beneficial for the rapid equilibration of the catalysts.

## Microreactor Evaluations

A fixed bed microreactor is used for catalytic evaluations. Analyses of the reactor feed gases prior to and after the reaction (including for butane and reaction products such as MA, acetic acid, and acrylic acid) are carried out by gas-liquid chromatography (GLC).

The pseudo first order rate constant,  $k$ , given for the disappearance of butane, is obtained by fitting the reactor data to a classical first order rate expression:

$$d[\text{butane}]/dt = -k[\text{butane}],$$

$$d(x_0 - x)/dt = -k(x_0 - x),$$

where  $x_0$  is the initial concentration of butane and  $x$  is the portion of butane reacted.

Integrating this expression gives the concentration of butane exiting the reactor as a function of contact time,  $t$ , in the reactor:

$$[\text{exit butane}] = x_0 - x = x_0 \exp(-kt).$$

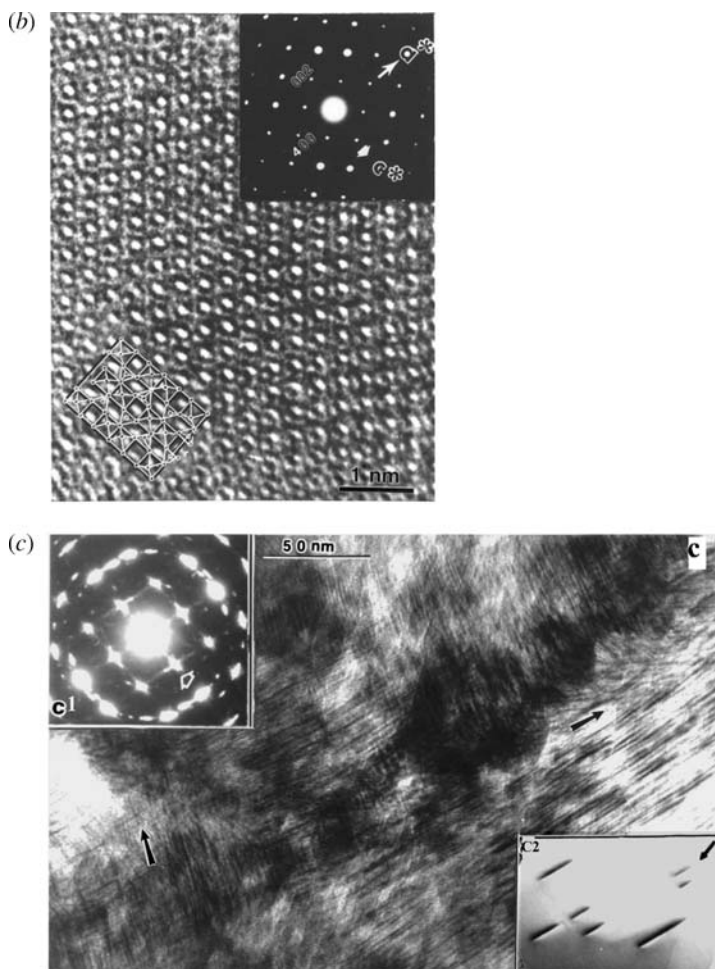
In addition to describing the reaction rate of butane with a catalyst, the rate constant,  $k$ , includes several other factors including the dependence of the reaction rate on the oxygen concentration (which remains relatively constant under our conditions) and the concentration of catalyst active sites (also assumed constant).

## In Situ ETEM Observation of Butane Oxidation

Direct in situ ETEM studies of dynamic butane oxidation over (010) VPO catalyst (Figure 2*b*) at operating temperatures ( $\sim 360$ – $390^\circ\text{C}$ ) are reported in *Science* (20).

**Figure 2** (b) Atomic resolution ETEM image of (010) VPO in butane. The associated electron diffraction (ED) is inset. The 002 and 400 Bragg reflections are shown along with the corner positions of 201 reflections. The structural model is approximately superimposed to illustrate vanadyl and P atom columns. The image and ED show a well-ordered structure. (c) In situ ETEM studies of VPO reaction in butane recorded at  $\sim 390^\circ\text{C}$ , showing two sets of extended defects along the symmetry related  $[201]$  and  $[20\bar{1}]$  directions, indicated by arrows. Inset (C2) shows one set of dynamic extended defects formed close to the catalyst surface, imaged in the 201 reflection in diffraction contrast. Inset (C1) shows the corresponding ED with diffuse streaks along  $\langle 201 \rangle$  indicating that  $\langle 201 \rangle$  planar oxygen atoms are partaking in the catalysis. (d) In situ ETEM of one set of the extended defects at high resolution showing a stacking fault close to the catalyst surface, bounded by partial screw dislocations P1 and P2 and lattice displacement along  $\langle 201 \rangle$ . (e) (*top*) A three-dimensional projection of a partial layer of the idealized (010) VPO structure showing oxygen atoms (along  $\langle 201 \rangle$ ). O and O' are in front and back layers. Some V and P atoms are denoted. (f) (*Bottom*) Generation of glide defects and model for novel glide shear mechanism along  $\langle 201 \rangle$  in butane oxidation catalysis. The atom shown by arrow (e.g., top of front layer) glides to the site created by loss of O and so on. Analysis of the extended defects, using electron microscopy, shows them to be formed by novel glide shear (18, 20). (g) A two-dimensional structural model for the observed extended glide shear plane defects that represent the diffusion front of anion vacancies: projection of one layer of the idealized (010) VPO, showing the novel glide shear mechanism. The glide defects accommodate misfit between the surface-containing anion vacancies (*filled circles*) and the underlying matrix and preserve anion vacancies associated with Lewis acid sites for catalysis. (h) Schematic of glide shear: glide plane defects at the interface between the catalyst surface-containing anion vacancies and the underlying matrix.

These studies have shown evidence for catalyst surface structure modifications accompanied by two sets of symmetry-related extended defects along  $\langle 201 \rangle$  directions (shown by arrows in Figure 2c in diffraction contrast). One set of the defects in the HRTEM image is shown in Figure 2d. Defect analysis reveals that the defects are formed by the glide shear mechanism (18, 20) shown in the structural model in Figure 2e–g. The defects are partial glide (screw) dislocations separating a stacking fault in  $\{201\}$  planes, and the stacking fault is terminated by the dislocation. In the defect mechanism, anion vacancies are formed in the basal plane along  $\langle 201 \rangle$ , between corner-sharing phosphate tetrahedra and vanadyl octahedra following the catalyst oxygen loss in the butane oxidation. This important glide shear process, in which oxide surface layers undergo a structural transformation by glide shear to accommodate the surface misfit owing to anion vacancies formed during the butane



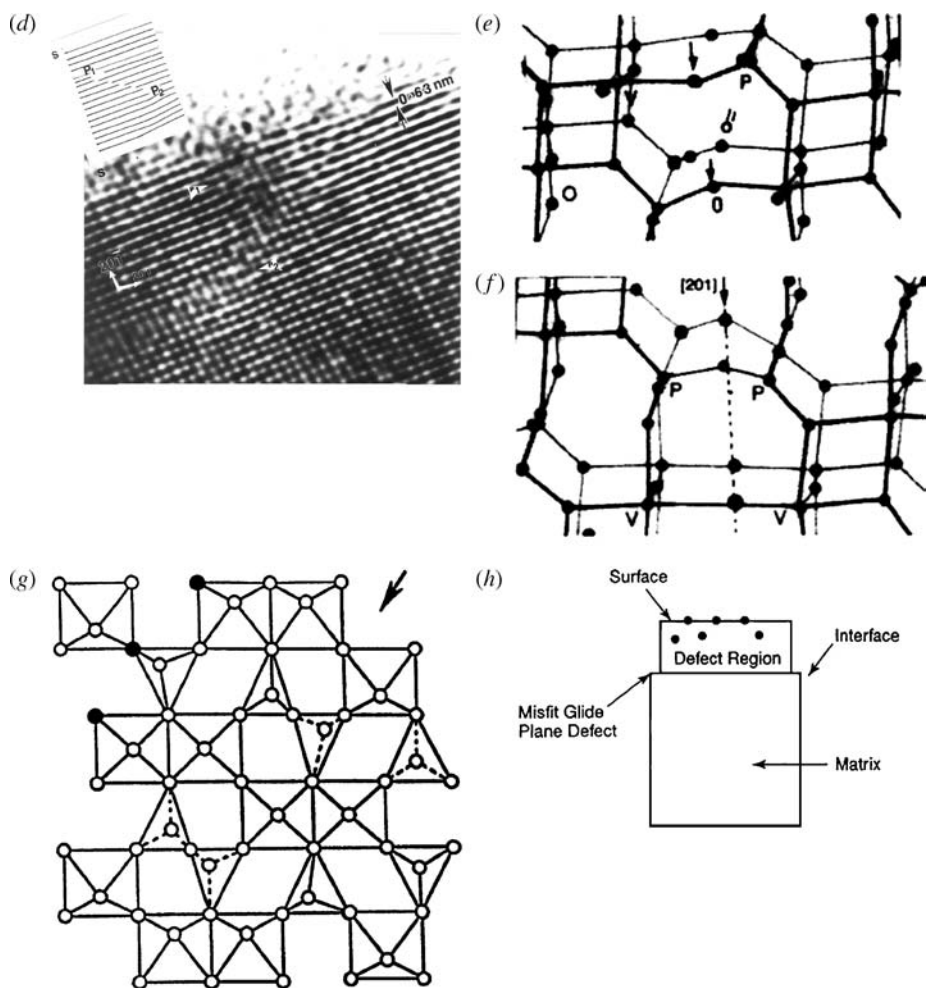


**Figure 2** (Continued)

reaction, essentially preserves anion vacancies associated with Lewis acid sites at the catalyst surface, as shown in the schematic in Figure 2h. This novel mechanism explains the release of structural oxygen and preservation of active Lewis acid sites without the catalyst structural collapse. The doubly positively charged anion vacancy sites are important in the hydrocarbon activation and oxygen exchange in the catalyst regeneration. The glide shear defect regions correspond to a slightly anion-deficient defect pyrophosphate phase, with pyrophosphate groups sharing corners similar to metaphosphate ( $\text{PO}_3$ )<sub>n</sub> groups. The local glide defects regions, which maintain the anion vacancies ( $\text{V}^{3+}$  phases), do not change the overall VPO structure under the catalyst-operating conditions and as such are not visible in X-ray diffraction (XRD). In situ ETEM and electron diffraction have

thus played a key role in unraveling the important defect structures in butane catalysis. The correlation of the glide defect microstructure with catalytic reactivity in hydrocarbon oxidation catalysis has shown uniformly high selectivity for MA in 1.5% butane/air in VPO for prolonged periods with maintenance of high reactivity in other catalytic oxides. These data indicate that glide shear is the most effective defect mechanism by which oxide catalysts accommodate nonstoichiometry and continue to operate in selective hydrocarbon oxidation reactions (18).

## Effect of Steam Exposure on the Catalyst Performance

In any hydrocarbon oxidation, steam/water vapor is a by-product. The effect of catalyst exposure to water vapor, especially on the catalyst microstructure and performance, remains a relatively unexplored area. The complex characteristics of long-term effects of water vapor and the evolution of defect structures have been described in the literature (35). In these studies, VPO catalysts are exposed to nitrogen/steam environments for periods ranging from 24 h to 312 h. Powder XRD has shown a modest decrease in diffraction line widths in samples treated for longer periods (312 h). ETEM shows that steam plays an important role in the development of glide defect structures in the catalyst. The key observation from in situ ETEM is the gradual evolution of the extended glide defects along  $\langle 201 \rangle$  orientations, with increased concentration compared with the concentration of defects in catalysts treated in nitrogen only. Prolonged steam exposure leads to a long-range order of the glide shear defects (18). In situ ETEM studies of reduction of VPO and other oxide systems have revealed the formation of extended glide shear defects, with the defect ordering leading to new homologous series of phases based on the crystal glide shear mechanism (18). The studies have important implications in oxide catalysis and, more generally, in oxide crystallography.

## EFFECT OF CATION PROMOTERS

In in situ studies of promoted catalysts, compositions of gases (e.g., 1.5% butane/air) in the ETEM microreactor are comparable to those in a practical reactor. In situ data are complemented by SEM, STEM with selected area electron diffraction, and EDX. In a recent study (36), both as-prepared powders and cross-sectioned samples (for compositional depth profile) were used to understand the differences in the surface and bulk composition of a number of promoted vanadyl pyrophosphate catalysts. The catalyst particles are cross sectioned to allow access to the surface and to the interior (core) to obtain insights into relationships between the promoted catalyst microstructure and the reactor performance. Vanadium oxidation state measurements, as determined by redox titrimetry, show small changes in vanadium oxidation state after activation. Likewise, large changes in  $N_2$ /BET surface area are not observed for these systems, suggesting that the increased n-butane oxidation activity is through modification of active sites or an increase in the site density (sites/m<sup>2</sup>) of the catalyst surface.

**TABLE 1** Fixed bed microreactor data in 2% butane/air, 380°C, of grafted catalyst systems compared to control catalysts

Catalyst composition	$k$ (s <sup>-1</sup> )	Selectivity at 40% conversion	Vox	N <sub>2</sub> /BET SA (m <sup>2</sup> /g)
(A) 1 mol% Bi, Mo VO(HPO <sub>4</sub> ) · 0.5 H <sub>2</sub> O	1.02	86	4.07/4.06	34
(B) 1 mol% Bi, Mo VO(HPO <sub>4</sub> ) · 0.5 H <sub>2</sub> O	0.88	83		
(C) EtOH on VO(HPO <sub>4</sub> ) · 0.5 H <sub>2</sub> O, precursor before activation	0.56	88	4.07/4.05	26
(D) HCl + EtOH on VO(HPO <sub>4</sub> ) · 0.5 H <sub>2</sub> O, precursor before activation	0.49	83		
(E) VO(HPO <sub>4</sub> ) · 0.5 H <sub>2</sub> O, precursor before activation	0.56	86	4.00/4.01	30

Powder XRD data of Bi, Mo-promoted catalysts, catalysts with ethanol alone and control catalysts, show single-phase crystalline vanadium pyrophosphate. Surface area and redox titrimetry data are listed in Table 1. Table 2 shows data for higher butane concentrations.

The tables show that improved reactor performance is observed for the grafted promoted VPO systems. The results of grafted catalysts have been compared with data from the coprecipitated promoter catalyst.

**TABLE 2** Fixed bed microreactor reactor, 2% butane/air, 9% butane/air at 380°C

Catalyst	2% Butane/air		9% Butane, 10% O <sub>2</sub>	
	$k$ (s <sup>-1</sup> )	Selectivity at 40% conversion	Yield	Selectivity
(1) Control catalyst	0.50	80	7.2	80
(2) 5BiMo	0.89	66	6.2	60
(3) 1BiMo	1.12	87	10	70
(4) Higher Bi	1.84	62	12.8	75
(5) Higher Bi, highest Bi/Mo ratio possible using anhydrous chloride alkoxides in EtOH	1.22	71	7.6	71
(6) Higher Mo	0.92	63	7.4	65
(7) Mo only	0.91	90	9.2	75
(8) 5 mol% Mo on VPO precursor	1.22	71	7.6	60

The catalyst systems (e.g., catalyst A) in Table 1 are prepared by reactive grafting of the mixed alkoxides of bismuth on molybdenum on preformed vanadium hydrogen phosphate precursor followed by calcination and activation at 460°C in 1.5% butane/air. In Table 1, fixed bed microreactor data obtained using a 2% butane/air feed mixture are shown. The catalyst activity of the catalysts grafted with 1 mol% of Bi, Mo after the calcination and activation heat treatments in 1.5% butane/air is shown for catalysts (A) and (B). Remarkably, the pseudo first order rate constant is approximately 60–80% greater than that of the untreated, control catalyst (catalyst E). N<sub>2</sub>/BET surface area measurements show nearly negligible changes in surface area, indicating that the performance improvements of the grafted systems are most likely related to an increase in the density of active sites on the catalyst. In either case, bismuth is a significantly beneficial cocatalyst and together with molybdenum greatly enhances catalyst activity while maintaining a high selectivity to MA. Bismuth may function to stabilize molybdenum (or vanadium) in a more stable and selective oxidation state, and this role may become more important under the more reducing conditions of the 9% butane/10% O<sub>2</sub> reactant stream (Table 2).

Microchemical depth profiling studies show that the catalyst surface layers are molybdenum rich, and the core of the catalyst particles are enriched in bismuth, in the 1 mol% Bi, Mo VPO catalyst. Figure 3 shows the compositional depth profile of the Mo/Bi ratio, plotted (with a scaling factor) as a function of depth in the

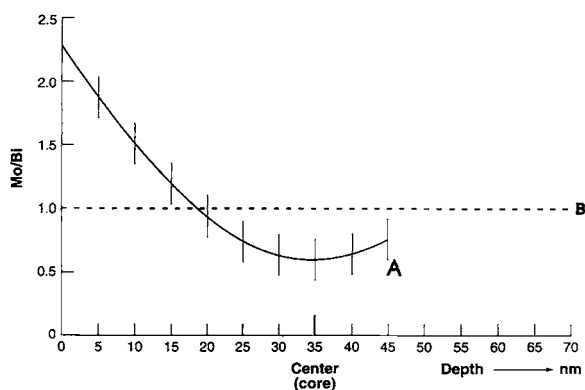


**Figure 3** Compositional depth profile of Mo/Bi ratios (scaled) plotted as a function of depth in the catalyst from the surface to the interior (core) of cross-sectioned samples. Plot A is for grafted 1 mol% (Bi, Mo) VPO catalyst and plot B is for catalyst prepared by coprecipitation of promoter cations with the precursor (coprecipitated catalyst). The grafted catalysts show surface enrichment of Mo and the core enrichment of Bi and higher reactivity and selectivity compared with coprecipitated catalysts. Statistical variations are shown. The coprecipitated catalyst (B) does not show this behavior.

catalyst crystal, from the surface to the center (interior) of the particles. Plot A shows the composition depth profile for the grafted catalyst 1 mol% Bi, Mo VPO, and plot B is the composition depth profile for coprecipitated (Bi<sub>0.05</sub> Mo<sub>0.05</sub>) VPO.

The presence of the Mo-rich phase may therefore be responsible for the observed enhanced catalytic activity, by altering the nature or introducing new active sites on the catalyst surface. As described previously (20), anion vacancies and glide defects are introduced in VPO following catalyst oxygen loss in butane oxidation, leading to V<sup>3+</sup> phases. It is believed that anion defect concentrations from the substitution of Bi<sup>3+</sup> are optimized by Mo<sup>6+</sup>, thus maintaining the optimal concentration of defects and surface vanadium oxidation state (36).

## FUTURE CHALLENGES IN ALKANE OXIDATION CATALYSIS

For VPO chemistry, a major challenge is to understand the nature of the equilibrated catalyst, the activation conditions for generating the equilibrated catalyst, and the effect of the catalyst compositional change on the catalyst activation. Large, parallel microreactor systems are probably best suited to investigating this large parameter space. Here too, in situ ETEM studies are set to play an important role to advance the field. In this section, the nature of anion vacancy defects, especially near the catalyst surface, and their marked effect on catalyst performance are reviewed. These vacancy defect structures may also be induced and perhaps stabilized by investigating catalyst/support interactions. These approaches may be crucial to creating advanced catalysts with higher productivities for this chemistry, as well as for other selective oxidations. Finally, it can be speculated that the stabilization of furan intermediate in the butane oxidation and its subsequent hydrogenation to THF (or THF in a single step) by overcoming the thermodynamically favorable MA production can have a huge economic impact.

## ELECTRON MICROSCOPY IN ENVIRONMENTAL CONTROL CATALYSIS

In this section we review the contributions of TEM techniques in three areas at the core of environmental catalysis: three-way catalysis (TWC), De-NO<sub>x</sub> catalysis, and catalysis for alternative, cleaner energy sources. These areas are, to a large extent, related, either through some of the reactions involved or through the formulation of the materials that are currently being employed or essayed in these catalytic processes. Thus although a TWC is actually the essential component of the emission control system of all the spark-ignited motor vehicles (42, 43), and De-NO<sub>x</sub> technology is well established for the after-treatment of nitrogen oxide emissions from stationary sources, future trends in engine concepts envisage these in combination. For instance, improved fuel economy and zero-CO<sub>2</sub> emissions

will require the development of after-treatment catalysts for automobiles, which should guarantee the efficient elimination of nitrogen oxides under lean-burn conditions (44–46). Likewise, in a recent prospective review on automotive catalysis by Shelef & McCabe (47), the replacement of actual fossil fuels by hydrogen has been outlined as one of the ways to mitigate the contribution of vehicular transport to the accumulation of CO<sub>2</sub>. Fuel cells and the combustion of methane from natural gas are pointed as the basis of these reduced CO<sub>2</sub>-emission alternatives (46, 47). A very recent publication (48) also stresses the close connection between the areas mentioned previously.

Although TWC and De-NO<sub>x</sub> processes for stationary sources are nowadays well-established technologies (2), further developments are still necessary to fulfill the more stringent emission limits of future legislation (i.e., EURO IV in 2005 and in the United States). For the TWC, extending the lifetime (mileage) of the catalytic converters up to 100,000 km is still a challenge that requires improvements in their deactivation behavior. Likewise, overcoming the problem of toxic emissions (mostly hydrocarbons) during the 30 s or so period of cold-start, in which the TWC catalyst temperature is not high enough to guarantee an efficient conversion of the pollutants in the exhaust gases, or the development of efficient catalysts for the reduction of nitrogen oxides under oxygen-rich (lean) conditions are some challenges that will likely require parallel developments from the materials side (47). Of course, this is also true for application in the field of catalysis for energy, in which interest in catalytic processes for in situ generation of H<sub>2</sub> for fuel cell applications has steeply risen recently.

As outlined above, the involvement of TEM in catalyst characterization and development can be categorized into three levels: (a) TEM is used as a routine tool to determine basic catalyst parameters, for example, TEM determination of particle size; (b) well established TEM techniques are exploited intensively to understand particular aspects of material chemistry problems in catalysis; and (c) novel EM techniques are applied to develop catalysts. These approaches are valuable in environmental catalysis, and below several examples are described. We comment on not only the most relevant results but also on suggestions about additional aspects of interest that could be potentially investigated by TEM.

It should be remembered that catalysts, owing to their usually complex formulation and their micro- or nanocrystalline nature, represent a bench-mark for most TEM techniques. In addition, TEM provides a unique view of these peculiar materials that most often is out of reach by any other macroscopic technique.

## TEM in Three-Way Catalysis

According to Shelef & McCabe (47) the union of catalysts and the automobile has been one of the greatest successes of heterogeneous catalysis over the past 25 years. TWC allows the oxidation of CO and unburned hydrocarbons into H<sub>2</sub>O and CO<sub>2</sub> and, simultaneously, the reduction of nitrogen oxides (NO<sub>x</sub>) into N<sub>2</sub>

(1) under air-to-fuel ratios (A/F) close to the stoichiometric point,  $A/F = 14.5$  (17). The actual formulation of these catalysts include (47) noble metals (Pt, Pd, Rh), redox (oxygen storage), textural promoters ( $CeO_2/Ce_xZr_{1-x}O_2$ ), an alumina support ( $\gamma-Al_2O_3$ ), and some alumina stabilizers such as lanthana, silica, or baria (2, 44, 49).

The contributions of EM to basic and applied knowledge on these types of catalysts have been focused on the following topics: (a) influence of synthesis procedures on the nanostructure of the catalysts; (b) understanding redox behavior; (c) metal-support interaction effects in noble metal/cerium-based oxides; and (d) understanding deactivation phenomena. Although they have been cited separately, these topics are, to an extent, related to each other. It is also important to state that most of the TEM work has been performed on TWC model systems consisting of noble metals (NM = Pt, Rh, Pd) supported on a variety of cerium oxides including pure ceria, Ce-Zr mixed oxides, Ce-Ln (Ln = Ce, Pr) mixed oxides, or more complex ternary or quaternary mixed oxides.

## NANOSTRUCTURE-SYNTHESIS CORRELATIONS AS SEEN BY TEM

In relation to synthesis, HRTEM has provided key information about the strong perturbation of the redox behavior of NM/Ceria systems associated with the use of chlorine-containing precursors (50–56). It has been suggested that the large amounts of chlorine incorporated into ceria or ceria-zirconia supports during impregnation and further activation in hydrogen result in the formation of a tetragonal-CeOCl phase, which grows in topotaxy with the ceria matrix. The stabilization of  $Ce^{3+}$  species in this crystalline phase perturbs and limits the extent of the  $Ce^{4+}/Ce^{3+}$  exchange process thus modifying the redox response of these materials (Figure 4).

Systematic approaches using TEM to establish the influence of synthesis procedures on the nanostructure of TWC or TWC model catalysts are lacking. In isolated contributions, TEM techniques are used to determine basic structural parameters such as the size of metal particles, the size of the oxygen storage or redox promoter crystallites, or some crystallographic features of the redox promoter component in Ce-Zr- and Ce-Tb-mixed oxides prepared using the microemulsion method (57–60).

Basic applications of TEM focused on the metal component can also be found in a number of papers. Bera et al. (61, 62) used TEM to investigate the effect of  $CeO_2$  in promoting CO oxidation and NO reduction reactions on Pt/ $CeO_2$  and Pd/ $CeO_2$  catalysts and found an atomically dispersed metallic phase in close contact with the support. HRTEM has been applied (63) to study the effect of the support in the dispersion of the metal phase in Rh catalysts. From comparison of particle-size histograms established from HRTEM images of an Rh/ $Ce_{0.5}Zr_{0.5}O_2$  and an Rh/ $Al_2O_3$  catalyst, the authors suggest that the mixed ceria-zirconia supports

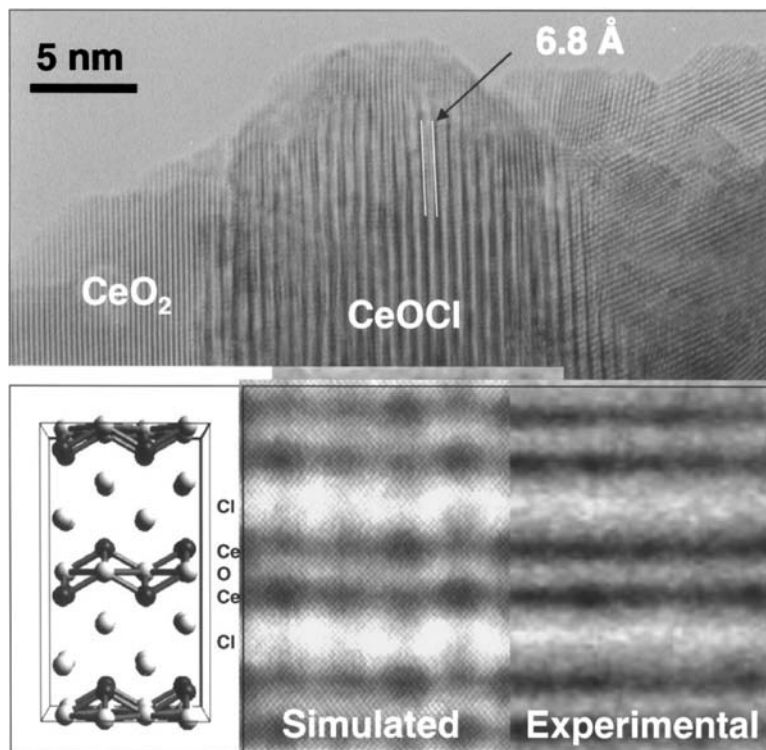


**Figure 4** (top) HRTEM image recorded on a Rh/CeO<sub>2</sub> catalyst prepared from a chloride Rh precursor. A t-CeOCl crystal imaged down [010] is observed. Notice the parallel alignment with respect to the CeO<sub>2</sub> matrix. (bottom) [010]-CeOCl structure, [010]-CeOCl-simulated image and enlargement of the experimental image.

stabilize a highly dispersed state of the metallic component of the catalyst, one of the roles commonly attributed to this component of TWC catalysts.

## TEM Studies of TWC Deactivation

One of the most valuable contributions of TEM in TWC has been in the deactivation of TWC catalysts. TWC catalysts work under harsh temperature and chemical environment conditions. A complex mixture of gaseous components whose redox character cyclically changes (at a frequency of about 10 Hz) between net oxidizing and net reducing, flows at a very high velocity over the catalyst at temperatures that can reach peaks of over 1000°C (2). Such redox and thermal stresses lead to severe modifications in the TWC converter.

The contribution of TEM to understanding the deactivation phenomenon refers to real as well as model TWC catalysts. Concerning the former, there is an interesting analytical EM study (BF-STEM and EDS analysis) on samples obtained

from an aged catalyst removed from a 34,800 Km-driven car (64). Using TEM techniques the authors conclude that there were many different deactivation factors. According to their results, loss of the metal components (Pt, Pd), changes of the alumina carrier, and Pt-Pd alloying effects were negligible, whereas metal particle sintering and poisoning by P, Pb, and S were the most important deactivation factors. These authors highlighted the role of TEM as an indispensable tool for the diagnosis of deactivation of TWC and point to the importance of TEM for determining metal particle size in real TWC catalysts deactivated by poisoning. In these samples, conventional adsorption measurements failed to establish this parameter due to complications in the chemisorption behavior of common probe molecules.

In relation to deactivation by poisoning, the contribution of cerium sulfate (64), cerium phosphate (65), and Pb-Al<sub>2</sub>O<sub>3</sub> compounds (42) formation have been studied using HRTEM and EDS analysis. Blockage of Ce<sup>4+</sup>/Ce<sup>3+</sup> redox exchange reaction by formation of stable Ce<sup>3+</sup> compounds and modification of the texture and surface acid-base properties of alumina are the likely origins of such deactivation. From TEM observations, Graham et al. (66, 67) noted the occurrence of a peculiar deactivation effect: encapsulation of Pd particles within the matrix of the redox promoter (a Ce<sub>0.5</sub>Zr<sub>0.5</sub>O<sub>2</sub> mixed oxide with a surface area of 88 m<sup>2</sup>/g in their studies). Aging at 1150°C in an atmosphere that mimics the exhaust gas conditions results in severe sintering of the Ce-Zr mixed oxide support (surface area drops down to 1 m<sup>2</sup>/g). TEM, ED, and elemental EDS analyses, performed on cut samples, convincingly prove the presence of large (50 nm) Pd-containing particles buried within the structure of the collapsed support (67). About 85% of the metal loading becomes encapsulated. According to the authors (66), the encapsulated particles suffer a compressive lattice strain (in the range of 1–3%).

Sintering of the metal particles is undoubtedly one of the key factors that contributes to TWC deactivation (64, 68–72). Systematic HRTEM studies of sintering of Pt and Rh catalysts supported on ceria-based oxides, in a variety of oxidizing and reducing atmospheres, have been performed by Bernal et al. (73–79). These studies, shown in Figure 5a, reveal that in general Pt is much more prone to suffer sintering at high temperature under reducing environments than does Rh. Sintering phenomena becomes especially significant for both metals at temperatures above 700°C. Also interesting, in the case of Rh catalysts sintered at high reduction temperatures (900°C), is that oxidation treatments at temperatures above 800°C produce the redispersion of the large Rh particles (80, 81). According to these authors, Pt behaves quite differently in this respect. In contrast to Rh data, HRTEM, EDS, and SEM data indicate that after high-temperature oxidation treatments, Pt particles supported on ceria sinter heavily into micron-sized metallic aggregates (76, 81), which coexist with a small fraction of 2–3-nm-sized Pt particles. Regarding the behavior of Pd, redispersion effects have been also invoked (82) to explain the reactivation of a Pd/Ce<sub>0.68</sub>Zr<sub>0.32</sub>O<sub>2</sub> catalyst, aged under real conditions, after oxidation at high temperature (900°C). Others conclude that metal loading does not have any influence on the sintering behavior. However, the transition of

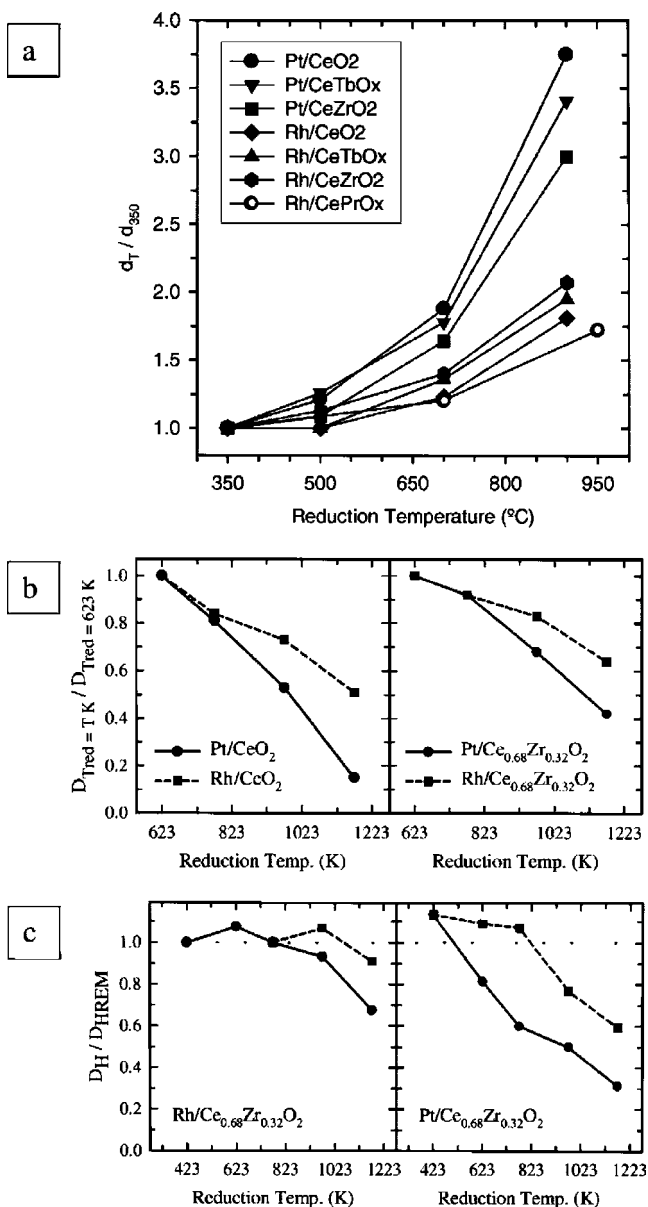


**Figure 5** (a) Evolution of average particle size as a function of reduction temperature ( $T_{\text{red}}$ ) for a series of Rh and Pt ceria-based catalysts. Data are referred to the average value at the lowest  $T_{\text{red}}$ . (b) Evolution of dispersion, as determined from HRTEM, as a function of  $T_{\text{red}}$  for two Rh and Pt catalysts. (c) Evolution with  $T_{\text{red}}$  of dispersion values determined from HRTEM ( $D_{\text{HREM}}$ ) and from volumetric  $\text{H}_2$ -chemisorption experiments ( $D_{\text{H}}$ ) for an Rh and a Pt catalyst supported on a ceria-zirconia mixed oxide.

alumina from the  $\theta$  to the  $\alpha$  polymorph seems to enhance the growth of the metal particles.

In a recent paper (83), where aging under real driving conditions and laboratory-scale aging tests under hydrothermal (reducing and oxidizing) conditions up to 1200°C were compared, a good correlation was found. This study also revealed that sintering is the primary deactivation factor before poisoning starts to be important. HRTEM has also become an indispensable tool to reliably estimate the dispersion of the metallic phase in TWC model catalysts, a key parameter to understand their performance (74, 84), as well as particle size distribution histograms.

Figure 5*b* plots a comparative HRTEM study of deactivation (loss of dispersion) behavior of Pt and Rh catalysts supported on CeO<sub>2</sub> and Ce<sub>0.68</sub>Zr<sub>0.32</sub>O<sub>2</sub> as a function of reduction temperature. Note how Pt deactivates more severely than Rh on both supports in terms of dispersion (54). Likewise, Figure 5*c* illustrates the effect of using (simultaneously) dispersion values determined from HRTEM ( $D_{\text{HRTEM}}$ ) and chemisorption ( $D_{\text{H}}$ ). Data plotted in this figure, which represent the variation of the ratio of these dispersion values as a function of reduction temperature, have been used to detect the on-set temperatures of metal-support interaction effects in Pt and Rh catalysts supported on ceria-zirconia-mixed oxides. According to these data, this temperature is much lower in the Pt catalyst. Moreover, these data also suggest that reversibility of these interaction effects is higher in the case of the Rh catalysts.

## Understanding Metal-Support Interaction Effects

Metal-support interaction effects are a crucial factor for understanding the chemical and catalytic behavior of metal catalysts supported on ceria-based oxides because of the reducibility of these oxides. Metal-support interaction effects in the catalytic performance of noble metals (Pt, Rh, Pd) with ceria and ceria-mixed oxides in a wide range of reduction temperatures (200–900°C) have been the focus of a number of TEM studies (10, 54, 56, 57, 78–80, 85, 86–105). The epitaxial growth of the supported metal nanoparticles on the surface of the oxide supports is generally observed. Experimental and simulated HRTEM profile and plan-view images indicate that this growth takes place under two different kinds of orientation relationships: parallel and twined, Figure 6*a*. This is the most remarkable nanostructural feature of these systems after reduction at temperatures ranging from 200°C up to 700°C. Between 700–900°, reduced support moieties mobilize and migrate over the surface of the supported nanoparticles, which become “decorated” by crystalline support overlayers, Figure 6*b*. This decoration phenomenon has also been observed by HRTEM in other systems (12, 21, 22, 106). Recently, the role of these ceria overlayers in modifying CO adsorption, as well as in reactions involving CO or small hydrocarbons, has been investigated using model inverse systems (97, 104, 107). In the very-high-reduction temperature regime, 900°C or above, interaction between the metals and the support introduces more severe modifications (Figure 6*c*) and redispersion effects in supported Rh (Figure 6*d*), under oxidizing conditions. Thus alloying of the metals with the lanthanide

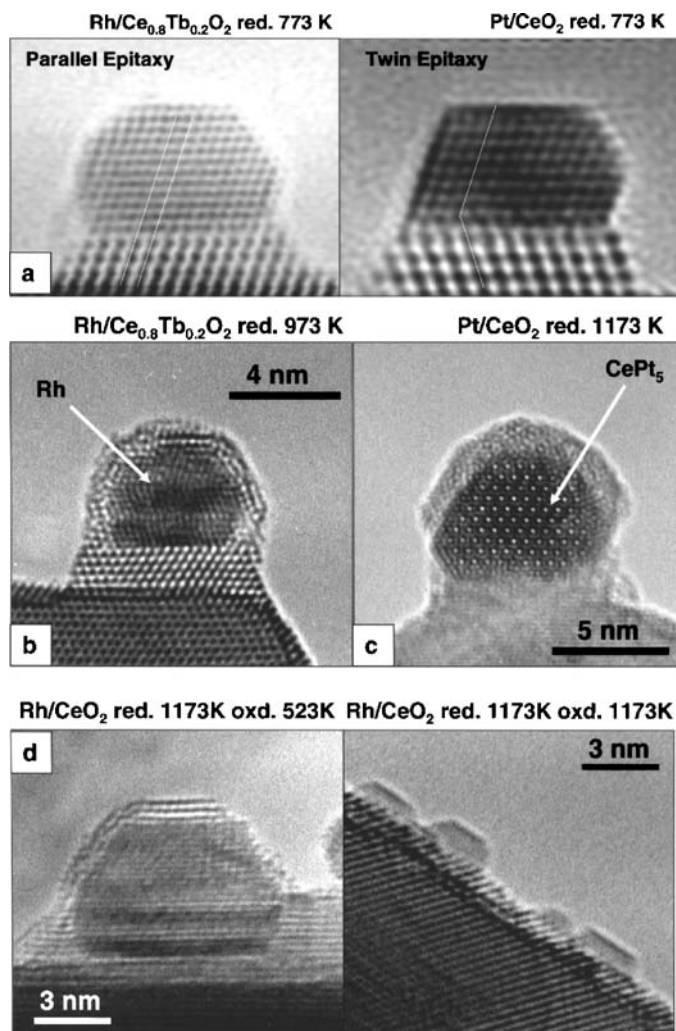


**Figure 6** Evolution of metal-support interaction effects, as revealed by HRTEM: (a) metal-support epitaxy; (b) decoration of metal particles; (c) Pt-Ce alloying; (d) reversibility of metal-support decoration effects (*left*). Redispersion of Rh into small, surface-clean, particles after oxidation at a high temperature of 1173 K (*right*).

elements present in the support (Ce in the case of pure ceria supports or Ce and Tb in the case of mixed Ce-Tb oxides) has been unambiguously detected by HRTEM and EELS. In the case of Pt, an LnPt<sub>5</sub> intermetallic (Ln = Ce or Ce,Tb) phase has been identified on the basis of ED and experimental and simulated HRTEM images, as well as by measuring directly the composition of supported nanoparticles in EELS spectra.

In the case of NM supported on CeO<sub>2</sub>-ZrO<sub>2</sub> mixed-oxides, appreciable differences are observed after reduction at the highest temperatures. Thus the extent of the decoration of Rh, Pt and Pd nanoparticles in samples reduced at 900°C is negligible compared with that observed on the catalysts based either on pure ceria or in mixed oxides containing two reducible lanthanides (Ce-Tb-mixed oxides). Likewise, the formation of intermetallic compounds has not been observed in Pt catalysts supported on Ce-Zr mixed oxides, whereas they have been clearly detected in Pt/CeTbO<sub>x</sub> systems. Therefore, the incorporation of zirconium into the ceria lattice seems to modulate the mobility of ceria, allowing ceria both to migrate over the particle surface and to diffuse into the fcc lattice of Pt.

In summary, the degree of metal-support interaction in NM/ceria catalysts increases with reduction temperature, going from purely structural interactions, through electronic interactions in the case of Pt, to metal-support interface rearrangements, and finally up to interactions that involve solid-state reactions between the supported phase and the support. TEM is a unique tool for unveiling the nanostructural features of metal-support interaction effects in TWC model catalysts, following their evolution in reducing and oxidizing environments as a function of temperature and, finally, indicating the precise temperature windows at which each type of manifestation appears or is removed.

## Contribution of TEM to the Understanding of Redox Behavior of TWC

One of the major roles of the ceria-based oxides added as redox promoters in TWC formulations is to damp the fluctuations of A/F ratios during the catalyst operation. By keeping this parameter as close as possible to the stoichiometric value, 14.5, the simultaneous elimination of the different pollutants present in the exhaust gases becomes optimum (2). Buffering the oscillations of the A/F is possible through the Ce<sup>4+</sup>/Ce<sup>3+</sup> redox exchange. This change in the oxidation state of cerium is accompanied by the creation/refilling of oxygen vacancies in the structure of the oxide. Among the roles attributed to the ceria oxides, we should also mention the promotion of CO conversion into CO<sub>2</sub> through the so-called water gas shift reaction (WGSR):  $\text{CO} + \text{H}_2\text{O} \rightarrow \text{CO}_2 + \text{H}_2$ . Such a promotional effect is also linked to the redox properties of these oxides.

The incorporation of zirconia or other reducible lanthanide elements into the ceria lattice significantly improves its redox behavior, which is one reason for substituting pure ceria with ceria-zirconia mixed oxides in the modern formulations of TWCs. Redox aging at high temperatures strongly modifies the redox properties of ceria-zirconia oxides. In the same way, the presence of a supported metal phase modifies the redox response of these oxides in a synergistic way, especially at low temperatures.

Structural and spectroscopic information available at atomic scale using TEM techniques provides key information for investigating this facet of TWC materials. Moreover, the recent achievement of atomic-resolution in situ TEM has opened

the extraordinary possibility of investigating the state of catalytic materials under conditions that avoid any alteration owing to their interaction with the oxidants present in atmospheric air, as well as following the dynamics of redox processes (5, 12, 48, 109, 110). This is an indispensable requirement for characterizing air-sensitive materials, as is the case for all NM/ceria catalysts.

Published TEM investigations of redox properties of TWC model catalysts encompass several topics: (a) monitoring changes in the oxidation state of the elements as a function of the chemical environment (110, 111); (b) understanding the way in which the oxygen vacancies are assimilated by the oxide (111); (c) elucidating the role of doping with other elements or the supported phase on the enhancement of the redox properties (112, 113); (d) unveiling mechanisms of modification of the redox response after high temperature redox aging (114–118); and (e) understanding the oxidation of the supported metal phases (80, 119–125).

The combined use of in situ EELS and in situ atomic resolution imaging of a Rh/Ce<sub>0.8</sub>Pr<sub>0.2</sub>O<sub>2</sub> catalyst under 5 torr H<sub>2</sub> pressure has been demonstrated as a function of temperature (25–900°C) (111). In situ HRTEM images obtained simultaneously with these spectra indicate that vacancies formed at low temperatures, associated to the reduction of Pr<sup>4+</sup>, did not order into superstructures, and ordering was observed once only when Ce<sup>4+</sup> began to become reduced. A  $\pi$  type phase, one of the members in the homologous series of reduced phases of the higher rare-earth oxides, has been detected in the mixed Ce-Pr oxide. Detailed analysis of HRTEM and in situ EELS spectra has allowed Sharma et al. to make semiquantitative estimations of the reduction degree in Ce-Zr mixed oxides as a function of reduction temperature and structural changes in Pr-Tb mixed oxides (110, 126, 127). Concerning the redox behavior of Ce-Zr-mixed oxides, HRTEM evidence has contributed to prove the formation of a twofold superstructure in these oxides after redox aging at high temperature (116–119). Such a superstructure could be on the basis of the enhanced oxygen storage and handling capabilities observed after such aging treatments (128, 129).

Detailed HRTEM studies are currently aimed at investigating the nanostructural changes of the supported metal phase upon treatments in redox cycles. The presence of a supported phase greatly modifies the redox response of the support. Hence, understanding the nanostructure of the metal phase becomes a requisite to characterize, in detail, the redox response of the whole system.

For Rh particles supported on silica, HRTEM evidence of the restructuring of large metallic particles, in the range of 5–10 nm in size, have been reported. Concerning the oxidation of Pd, complex nanostructural changes during the PdO  $\leftrightarrow$  Pd transformation have been revealed by the HRTEM images, which are used to rationalize the activity change pattern characteristic of Pd in complete oxidation reactions (124, 125). It is also worth highlighting, from the possibilities offered by TEM techniques in catalysts characterization, that the electron holography results obtained by Allard et al. (130) show evidence of the formation of internal voids at the core of Pd particles submitted to oxidation-reduction cycles.

## TEM of DeNO<sub>x</sub> Catalysts

Nowadays DeNO<sub>x</sub> catalysis encompasses the abatement of nitrogen oxide present in burnt gases emitted from stationary sources (power plants, chemical plants) and the control of NO<sub>x</sub> emission from automobiles working under oxygen-rich (lean) conditions. The catalytic technology in the former case, which is currently well established, is based on V<sub>2</sub>O<sub>5</sub> (MoO<sub>3</sub>-WO<sub>3</sub>)/TiO<sub>2</sub> formulations (2, 131). On these catalysts, the selective catalytic reduction (SCR) of nitrogen oxides using ammonia as reductant allows their total elimination in the presence of a large excess of oxygen.

In the case of automobiles, to date a large number (literally hundreds) of catalysts has been studied, but the ideal solution has not yet been found. SCR of NO<sub>x</sub> using different types of reductants (ammonia, urea, hydrocarbons) have been assayed on two kinds of materials: metal/zeolites and metal/alumina. A suitable solution of using a NO<sub>x</sub> storage system (NO<sub>x</sub>-trap) combined with a TWC catalyst has also been reported. In this case, during the NO<sub>x</sub> storage lean cycle, NO is oxidized into NO<sub>2</sub> on the TWC catalyst at the same time that residual CO and HC are oxidized and stored as a nitrate on a barium-containing compound. Then, for a few seconds, the engine is operated under rich conditions, which allows the reduction of NO<sub>x</sub> into N<sub>2</sub> and the regeneration of the trap.

Although TEM has not been used as intensively on these materials as has TWC, relevant contributions to understanding their performance and deactivation can be found in recent literature dealing with V<sub>2</sub>O<sub>5</sub>/TiO<sub>2</sub> systems (132–136), M/Al<sub>2</sub>O<sub>3</sub> [M = Ag (137–139), Pd (140, 141), Cu (142), Pt (143), Re (144, 145)], and M/zeolite (146–149) catalysts.

## TEM of V<sub>2</sub>O<sub>5</sub>/TiO<sub>2</sub> Catalysts and Related Systems

The influence of the synthesis procedure on the nanostructure of V<sub>2</sub>O<sub>5</sub>/TiO<sub>2</sub>-type catalysts has been investigated (134, 136). Reddy et al. (134), using HRTEM and EDS, studied the promoting effect of ZrO<sub>2</sub> in a V<sub>2</sub>O<sub>5</sub>/ZrO<sub>2</sub>-TiO<sub>2</sub> catalyst and the role of calcination temperature on the structure of this catalyst. The transition from an amorphous TiO<sub>2</sub>-ZrO<sub>2</sub> support to a crystalline ZrV<sub>2</sub>O<sub>7</sub> compound, as the V-containing phase, dispersed on the surface of the TiO<sub>2</sub>-ZrO<sub>2</sub> support, is detected as the calcination temperature is raised from 500°C up to 800°C. A critical 4% V<sub>2</sub>O<sub>5</sub> loading is reported to establish the nature of vanadia-titania interaction in catalysts, which were prepared using the sol-gel route (136). For loading below this limit, HRTEM images suggest that vanadia exists in the form of titania-coordinated surface species, whereas for loading higher than 4%, three-dimensional hexagonal V<sub>2</sub>O<sub>5</sub> crystallites, which are less active, are detected. The authors also claim that important changes in selectivity to N<sub>2</sub> in the SCR of NO by propane are linked to such nanostructural changes.

Deactivation phenomena have been reported (132, 133). EDS-TEM studies point out the interest in these techniques as deactivation diagnosis tools in the

V<sub>2</sub>O<sub>5</sub>-WO<sub>3</sub>-TiO<sub>2</sub> SCR European standard catalyst (EUROCAT) (132). After aging in real conditions, important changes in the distribution of V and W were detected that led to the formation of particles. The structure of the vanadia-tungsta surface coating suffers an amorphization process, and sulfur is detected as the major poison. EDS studies, performed on commercial SCR catalysts and reported in Reference (133), indicate that HCl also has some detrimental impact on V, facilitating its loss by formation of volatile species.

Dynamic redox phenomena and evolution of shear structures in vanadium pentoxide catalysts using in situ ETEM have been reported by Gai (150). EELS studies of the oxidation states of V in its oxide compounds have been reported that help to explain the catalytic performance and deactivation routes (151–154). The exceptional increase in energy resolution facilitated by the use of gun monochromators and improved, aberration-corrected-EELS spectrometers enables the EELS spectra to be brought down to about 0.1 eV, thus allowing fruitful comparative studies between experimental EELS spectra and theoretical electronic states obtained from band-structure calculation. Therefore, high resolution EELS will play an important role in the characterization of this family of catalysts in the near future.

### TEM Characterization of M/Al<sub>2</sub>O<sub>3</sub> De-NO<sub>x</sub> Catalysts

Concerning the nature of the active phase in M/Al<sub>2</sub>O<sub>3</sub> catalysts, Reference (142) provides an example of the simultaneous application of HAADF and EELS to characterize the spatial distribution of oxidation states of the metallic component. The presence of Cu in different oxidation states on the surface and bulk of the Cu particles, even after reduction at 800°C, is evidenced in a Cu/ $\gamma$ -Al<sub>2</sub>O<sub>3</sub> catalyst and attributed to the metal-support interaction effect. HRTEM is used to elucidate the formation of a new La-Al<sub>2</sub>O<sub>3</sub> crystalline phase in Pd/Al<sub>2</sub>O<sub>3</sub>-La<sub>2</sub>O<sub>3</sub> catalysts (140) and the redispersion role of Re in high-temperature oxidation treatments of Re/ $\gamma$ -Al<sub>2</sub>O<sub>3</sub> catalysts (144, 145).

### TEM Characterization of M/Zeolite De-NO<sub>x</sub> Catalysts

Both the size and shape of the metallic component and its precise spatial distribution are essential parameters in the case of metal/zeolite systems. The location of the supported metal phase on the outer surface of the zeolite, or within its pore structure, can dramatically influence the intrinsic properties of the metal particles, due to a confinement effect, and also the course of the reaction within the pores. This is, therefore, an important parameter to be disclosed in this particular kind of material. For such a purpose, electron tomography becomes an indispensable tool (156). The first demonstration of three-dimensional characterization of catalysts, using bright-field (BF) tomography, is from Koster et al. (157). From a three-dimensional TEM reconstruction of an Ag/NaY catalyst, they conclude convincingly the presence of larger silver particles outside the channel structure and small ones (about 18 nm) inside the pores. With the same approach, they obtain precise information on the characteristics of pore structure and connectivity of the pore system in

zeolite Y (158). Also in an inspiring work, a detailed localization of silver particles and  $\text{ZrO}_2$  in SBA-15 zeolite is carried out (159). From the BF-tomography data, an interpretation of the hysteresis effects observed in the  $\text{N}_2$  desorption isotherms of this material is proposed.

More recently, HAADF STEM tomography has been introduced (160) and applied to catalyst characterization (161, 162). The direct Z dependence of this imaging mode allows fulfillment of the projection requirement of tomography. Using this new approach, partitioning of Pd-Ru bimetallic particles between the outer and inner surfaces of a MCM-41 zeolite has been nicely determined. Accordingly, the presence of nanoparticles at the zeptogram level of quantity can be imaged within mesoporous hosts (162). Backscattered imaging in a low-voltage SEM is shown to yield images of catalyst nanoparticles similar to STEM-HAADF images, which has economical advantages (5, 14, 163). HAADF imaging, in combination with EDS elemental mapping, has also proved of interest in unveiling deactivation mechanisms of a Pt/mordenite catalyst, under real operating conditions, in the SCR of  $\text{NO}_x$ -using ammonia (135). Analytical data evidence in this case is the preferential association of S with the Pt particles.

Finally, we will mention the results presented in Reference (146). There, HRTEM is used to characterize the geometrical arrangement of pores in a mesoporous Tin(IV) phosphate. The phosphate, with a hexagonal arrangement of the pores, appears more active than that which has a square distribution of the pores. HRTEM also allows the authors to draw conclusions about the amorphous nature of the pore walls, whose composition and Sn/P ratio were established from EDS measurements.

In summary, as shown with different examples, the array of TEM techniques has provided indispensable tools to understand synthesis, activation, performance, and deactivation of the different families of materials nowadays involved in De- $\text{NO}_x$  catalysis.

## THE ROLE OF TEM IN THE CHARACTERIZATION OF CATALYSTS FOR ALTERNATIVE ENERGY SOURCES

Reducing dependence on fossil fuels, diversifying energy sources, and reducing the environmental impact of current energy-producing processes are major targets of research in the field of catalysis for energy. A variety of processes are currently being investigated, among which those related to the production of  $\text{H}_2$  to feed fuel cells are most in focus. Reforming and partial oxidation of different raw chemicals as  $\text{CH}_4$ , methanol, or ethanol provide suitable ways to obtain  $\text{H}_2$  (164). Combustion of this  $\text{H}_2$  in a fuel cell would allow the transformation of chemical energy into electrical energy (165). Likewise, gasification of biomass into syngas ( $\text{CO} + \text{H}_2$  mixture) seems a viable alternative (166, 167).

Most of the TEM work related to catalysis for energy deals with the nanoscale characterization and development of materials (*a*) as catalysts in the electrodes

(anodes/cathodes) of fuel cells (168–172); (b) in the production of hydrogen via reforming with water (steam reforming) (173, 174) or with CO<sub>2</sub> (dry reforming) (175); (c) in the partial oxidation of CH<sub>4</sub> or ethanol (176–179); (d) in the low-temperature water gas shift reaction (180–182); and (e) in the selective CO oxidation in presence of H<sub>2</sub> (PROX process) (183–190).

The use of TEM in the characterization of electrode catalytic components is usually associated with the determination of metal particle size (168, 169), the evolution of particle size during the work of the electrochemical cells (172), or the degree of mixing of different metallic components in the case of bimetallic catalysts (170, 171). In the last case, EDS information is the key to detect alloy formation.

Catalysts for the production of hydrogen using ethanol as a starting point, via steam reforming or partial oxidation reactions, have been characterized with HRTEM. Thus in an extensive study of Co catalysts supported on a varied set of supports (174), ED and HRTEM imaging provide key information to identify the possible nature of the phases in which Co is present under reaction conditions, by analyzing a series of samples after reaction. HRTEM images also provide information about the nature of the carbon deposits, formed on the catalysts, which contribute to the catalyst deactivation.

Rh/CeO<sub>2</sub> has been very recently highlighted, in a report that appeared in *Science*, as a candidate to obtain H<sub>2</sub> from ethanol via an autothermal reaction process (191). This system appears active, and has potential practical applications in the gasification of biomass (166, 167). TEM knowledge developed around this type of catalyst becomes of renewed interest in the light of these extraordinary findings.

Also in the field of cerium oxides, we should recall the HRTEM work performed by Kang et al. (178) and Kang & Eyring (179) in the characterization of binary, Ce-Zr, Fe-Ce, ternary Ce-Zr-Tb, and more complex Ce<sub>1-x-y-z</sub>Pr<sub>x</sub>Tb<sub>y</sub>M<sub>z</sub>O<sub>2-δ</sub> (M = lanthanide element, Zr, Bi, Co, Mn, Cu, Pd, Ag, Ti, V, Nb, Mo, Ta, Fe) mixed oxides. On the basis of these oxides, the authors have submitted a patent (192) to produce H<sub>2</sub> in a continuous way, using a two-step cyclic process that involves the consecutive reaction of the oxides with CH<sub>4</sub> and then H<sub>2</sub>O (177). HRTEM imaging has been used in this case to understand the role of Fe in the enhanced reactivity of these oxides. Profile images have revealed the absence of carbon residues on the surface of the oxides after reaction and at the same time suggested an enrichment of Fe on the outer surface layers (179). Likewise, using HRTEM these authors have determined an enrichment in Ce at the surface of Ce-Zr-mixed oxides, which were treated using the so-called chemical-filing process (178). This enrichment would help to explain the improved low-temperature redox activity of Ce-Zr-mixed oxides after such chemical-filing treatment.

Ni/La<sub>2</sub>O<sub>3</sub> systems have also received attention as interesting catalysts in steam reforming of ethanol (193), catalytic partial oxidation of ethanol (176), and dry reforming of natural gas (CH<sub>4</sub>) (175, 194). The outstanding stability of this

catalyst, i.e., resistance to carbon deposition, has been attributed to the presence of La species on the surface of the Ni particles. In connection with this material, it is worth recalling the detailed HRTEM work developed by Bernal et al. on the preparation of metal/4f sesquioxide catalysts and the origin of metal-support interaction effects in this type of material (195–197). In agreement with HRTEM images reported in these papers, metal particles are decorated by lanthana patches after reduction even at low temperature. From detailed experiments and HRTEM observations, these authors evidence that such decoration effects take place during the impregnation of lanthana with the metal precursor, as a consequence of extensive dissolution of lanthana and ulterior coprecipitation with the metal precursor. Disclosing the occurrence of this process has been possible only on the basis of HRTEM imaging. Likewise, the formation of different lanthana phases [ $\text{La}_2\text{O}_2\text{CO}_3$ ,  $\text{La}(\text{OH})_3$ , lanthana perovskites], claimed to play some role in the reaction previously mentioned, have been detected and characterized by HRTEM in different steps of the preparation of these catalysts.

The ability of lanthana to reduce the metal particle size, in the case of the Ru/ $\text{La}_2\text{O}_3$  WGSR catalysts studied by HRTEM (180), is very likely also related to the formation of lanthana patches on top of Ru surfaces. The selective oxidation of CO in the presence of large amounts of hydrogen, also called the PROX reaction, is currently the focus of intense research activity. Removing CO from reformat gases, to levels below 5 ppm, is a crucial step in the use of  $\text{H}_2$  in fuel cells because the typical anode electrodes used in these cells are extremely sensitive to poisoning by CO. Gold-based catalysts seem good candidates to perform CO conversion at low temperatures. In fact, since the findings reported by Haruta et al. (198) about the remarkable activity of Au/ $\text{TiO}_2$  catalysts in the CO oxidation reaction, even at temperatures below  $0^\circ\text{C}$ , preparation and characterization studies of supported gold catalysts have received renewed interest.

Given that a small particle size ( $<10$  nm) is one of the key factors in the enhancement of the catalytic activity of gold (199), EM techniques are necessary to understand the catalytic properties of these materials. Thus TEM investigation of gold catalysts supported on different oxides can be found in recent literature, not only in connection with CO oxidation (183–187, 189, 190, 200–203) but also in other environmental catalysis applications such as oxidation of volatile organic compounds (VOCs) (204) or wet air oxidation of organic residues in waste waters (205).

Although most of the TEM work (185–187, 190, 204, 205) deals with the use of conventional TEM, BF, or HRTEM images to determine particle size and to clarify the influence of the synthesis methods and activation conditions on metal particle size distribution, some more detailed studies also have been reported. Thus HRTEM and EDS have been used to confirm the metallic state of gold in an Au/ $\text{FeO}_x/\text{C}$  catalyst after synthesis and also after reaction in CO oxidation catalytic assays (184). In this paper,  $\text{FeO}_x$  was determined, from HRTEM observations, to be present in the catalyst in the form of  $\text{Fe}_2\text{O}_3$ . In the case of Au/ $\text{CeO}_2$  catalysts,

HRTEM has revealed (183) the occurrence of surface reconstruction phenomena during CO oxidation.

Especially remarkable are the TEM studies conducted in a series of papers by Akita et al. (189, 200–203) on Au/TiO<sub>2</sub> catalysts. HRTEM performed by these authors has revealed the presence of epitaxial growth of the gold particles on top of the titania polymorphs (189, 202). ADF-STEM images and EELS data also reveal the preferential deposition of gold on the surface of the rutile polymorph (189). The systematic combined application of HRTEM and electron holography used by these authors to understand the influence of particle size on the morphology of the gold particles and on the features of the Au-titania interface is inspiring. Changes in the contact angle between the metal and the support are determined to take place at particle sizes about 2 nm. The mean inner potential of the small Au particles, which is another parameter determined by these authors from the electron holograms, shows significant deviations from the values corresponding to bulk gold, a fact that could really be at the origin of the peculiar catalytic behavior of the small Au particles. Moreover, changes with size of this mean inner potential are measured, which can be taken as an indication of the occurrence of charge transfer effects, i.e., of metal-support interaction effects (200, 201, 203). These papers highlight the tremendous potential of the HRTEM-electron holography in tandem in catalysts characterization.

## CONCLUSION

Herein we have commented on a significant numbers of papers dealing with the characterization and development of a large variety of catalytic materials using electron microscopy methods. A fully comprehensive survey of the use of EM techniques in such a widespread collection of catalysts has not been our main target. We have tried, instead, to present a collection of papers that adequately illustrate and represent the full potential of this large family of techniques in understanding and developing the catalysis of hydrocarbon oxidation, environmental protection, and energy.

A wide range of information is available because of electron microscopy, which opens a unique window to the intricate field of the structure and its relationship to reactivity of complex catalytic solids. Such information has established a guiding light in the synthesis of new catalysts with improved performances and the development of new processes and has provided a key to understanding the function and deactivation of catalysts.

## ACKNOWLEDGMENTS

We thank L.G. Hanna, F. Gooding, and L. Wang of DuPont (CRD) for technical support, and K. Kourtakis (DuPont), S. Bernal (Cadiz), and A.J. Pérez-Omil (Cadiz) for helpful discussions.

The Annual Review of Materials Research is online at  
<http://matsci.annualreviews.org>

## LITERATURE CITED

1. Thomas JM, Thomas WJ. 1997. *Principles and Practice of Heterogeneous Catalysis*. Weinheim, Ger.:VCH
2. Ertl G, Knözinger H, Weitkamp J. 2004. *Handbook of Heterogeneous Catalysis*. 4:559–696. Weinheim, Ger.: Wiley-VCH
3. Hirsch PB, Howie A, Nicholson RB, Pashley DW, Whelan MJ. 1977. *Electron Microscopy of Thin Crystals*. New York: Krieger
4. Williams DB, Carter CB. 1996. *Principles of Electron Microscopy*. New York: Plenum
5. Gai PL, Boyes ED. 2003. *Electron Microscopy Heterogeneous Catalysis*. Bristol/Philadelphia: Inst. Phys. Publ.
6. Zeitler E, ed. 1990. Monographic issue: characterization of catalysts. *Ultramicroscopy* 34:1–128
7. Gai PL. 1992. Defects in oxide catalysts: fundamental studies of catalysis in action. *Catal. Rev. Sci. Eng.* 34:1–54
8. Datye AK, Smith DJ. 1992. The study of heterogeneous catalysis by HRTEM. *Catal. Rev. Sci. Eng.* 34:129–78
9. Ledoux MJ, ed. 1995. Monographic issue: HREM for catalysis. *Catal. Today* 23:161–298
10. Bernal S, Baker RT, Burrows A, Calvino JJ, Kiely CJ, et al. 2000. Structure of highly dispersed metals and oxides: exploring the capabilities of high-resolution electron microscopy. *Surf. Interface Anal.* 29:411–21
11. Thomas JM, Terasaki O, Gai PL, Zhou W, Gonzalez-Colbet J. 2001. Structural elucidation of mesoporous and microporous solids using HRTEM. *Acc. Chem. Res.* 34:583–93
12. Gai PL. 2002. Development of environmental electron microscopy and applications to catalysis. *Top. Catal.* 21:161–74
13. Thomas JM, Terasaki O. 2002. The electron microscope is an indispensable instrument for the characterization of catalysts. *Top. Catal.* 21:155–59
14. Midgley PA, Weyland M, Thomas JM, Boyes ED, Gai PL. 2002. Electron tomography. *Angew. Chem. Int. Ed.* 41:20–25
15. Datye AK. 2003. Electron microscopy of catalysts. *J. Catal.* 216:144–54
16. Thomas JM, Gai PL. 2004. Electron microscopy and the materials chemistry of catalysts. *Adv. Catal.* 48:171–227
17. Thomas JM, Midgley PA. 2004. High-resolution transmission electron microscopy: the ultimate nanoanalytical technique. *Chem. Commun.* 253–67
18. Gai PL. 1997. A new structural transformation mechanism in catalytic oxides. *Acta Cryst. B* 53:346
19. Boyes ED, Gai PL. 1997. Environmental high resolution microscopy and applications to chemical science. *Ultramicroscopy* 67:219–32
20. Gai PL, Kourtakos K. 1995. Solid state defect mechanism in vanadyl pyrophosphate catalysts: implications for selective oxidation. *Science* 267:661–63
21. Gai PL. 1998. Direct probing of gas molecules-solid catalyst reactions at the atomic scale. *Adv. Mater.* 10:1259–63
22. Gai PL. 1999. Environmental high resolution electron microscopy of gas-catalyst reactions. *Top. Catal.* 8:97–114
- 22a. Gai PL. 1999. Probing selective oxidation catalysis under reaction conditions by atomic scale environmental high resolution electron microscopy. *Curr. Opin. Solid State Mater. Sci.* 4:63–73
- 22b. Gai PL. 2001. Development of electron microscopy methods in the study of

- catalysts. *Curr. Opin. Solid State Mater. Sci.* 5:371–80
23. Haggin J. 1995. Catalysis at the atomic level. *C&E News* 73:39–41
24. Jacoby M. 2002. EM in catalysis. *C&E News* 80:26
25. Gai PL. 2002. Development of wet-ETEM in catalysis. *Microsc. Microanal.* 8:21–28
26. Gai PL, Kourtakis K, Boyes E. 2005. In situ wet nanoscale imaging of nitriles in a solution phase: novel hydrogenation chemistry through nanocatalysts on nano-supports. *Catal. Lett.* 102:(1–2). In press
27. Crewe A. 2000. STEM. *Rev. Sci. Instr.* 42:411
28. Boyes ED. 1998. High resolution, low voltage SEM. *Adv. Mater.* 10:1277–80
29. Boyes ED. 2001. High resolution low voltage SEM and analysis. *Inst. of Phys. Conf. Ser.* 168:115–17
30. Boyes ED, Ringnalda J, van der Stam MA, Fliervoet TF, Van Cappellen E. 2001. A 2-2-2 200 kV field emission STEM/TEM system. *Microsc. Microanal.* 7:232–33
31. Midgley PA, Thomas JM, Laffont L, Weyland M, Raja R, et al. 2004. Electron tomography. *J. Phys. Chem. B* 108:4590–92
32. Centi G, ed. 1993. Monographic issue: butane catalysis. *Catal. Today* 16:1–193
33. Sananes MT, Hutchings GJ, Volta J. 1995. VPO catalysts. *J. Catal.* 154:253–60
34. Bordes E. 1993. V-P-O systems. *Catal. Today* 16:27–42
35. Gai PL, Kourtakis K, Coulson R, Jacobsen I. 1997. HRTEM of butane oxidation catalysis and correlation with reaction chemistry. *J. Phys. Chem.* 101:9916–25
36. Kourtakis K, Gai PL. 2004. Novel microstructures and reactivity in n-butane oxidation: advances and challenges. *J. Mol. Catal.* 220:93
37. Bartley JK. 2001. Vanadium phosphate prepared using solvent-free method. *Catal. Lett.* 3:99–105
38. Haber J, Zazhigalov V, Stoch J, Bogutskaya L, Batcherikova I. 1997. Mechanochemistry: the activation method of VPO catalysts for n-butane partial oxidation. *Catal. Today* 33:39–49
39. Hutchings GJ, Sananes MT, Sajip A, Kiely CJ, Burrows A, et al. 1997. Improved methods of preparation of vanadium phosphate catalysts. *Catal. Today* 33:161–71
40. Hutchings GJ, Higgins R. 1996. Promoted VPO catalysis. *J. Catal.* 162:153–60
41. Irusta S, Boix A, Pierini B, Caspani C, Petunchi J. 1999. Catalysis. *J. Catal.* 187:298–302
42. Magnacca G, Morterra C. 2000. Surface characterization of modified aluminas. *Phys. Chem. Chem. Phys.* 2:3903–8
43. Sung S, Smaling RM, Brungard NL. 1998. Pb poisoning on Pd-only TWC catalysts. *Stud. Surf. Sci. Catal.* 116:165–74
44. Farrauto RJ, Heck RM. 1999. Catalytic converters: state of the art and perspectives. *Catal. Today* 51:351–60
45. Gandhi HS, Graham GW, McCabe RW. 2003. Automotive exhaust catalysis. *J. Catal.* 216:433–42
46. Pishinger S. 2004. The future of vehicle propulsion—combustion engines and alternatives. *Top. Catal.* 30/31:5–16
47. Shelef M, McCabe RW. 2000. Twenty-five years after introduction of automotive catalysts: what next? *Catal. Today* 62:35–50
48. Wu JCS, Wan B-ZE. 2004. Catalysis for new energy resources and environmental protection. *Catal. Today* 97:93–215
49. Kaspar J, Fornasiero P, Hickey N. 2003. Automotive catalytic converters: current status and some perspectives. *Catal. Today* 77:419–28
50. Fornasiero P, Hickey N, Kaspar J, Dossi C, Gava D, Graziani M. 2000. Redox and chemisorptive properties of ex-chloride and ex-nitrate Rh/Ce<sub>0.6</sub>Zr<sub>0.4</sub>O<sub>2</sub> catalysts: 1. Effect of low-temperature redox cycling. *J. Catal.* 189:326–38
51. Fornasiero P, Hickey N, Kaspar J, Montini T, Graziani M. 2000. Redox and chemisorptive properties of ex-chloride and ex-nitrate Rh/Ce<sub>0.6</sub>Zr<sub>0.4</sub>O<sub>2</sub> catalysts:

2. Effect of high-temperature redox cycling. *J. Catal.* 189:339–48
52. Trovarelli A, Dolcetti G, Leitenburg C, Kaspar J, Finetti P, Santoni A. 1992. Rhodium-ceria interaction induced by high-temperature reduction: characterization and catalytic behavior in transient and continuous conditions. *J. Chem. Soc. Faraday Trans.* 88:1311–14
53. Le Normand F, Hilarie L, Kili K, Krill G, Maire G. 1988. Catalytic reactions. *J. Phys. Chem.* 92:2561–68
54. Bernal S, Botana FJ, Calvino JJ, Cauqui MA, Cifredo GA, et al. 1993. Microstructural and chemical-properties of ceria-supported rhodium catalysts reduced at 773 K. *J. Phys. Chem.* 97:4118–23
55. Bernal S, Botana FJ, Calvino JJ, Cifredo GA, Omil JAP. 1993. HREM study of the phases resulting from the preparation of ceria supported rhodium catalysts. *Electron Microsc. Anal.* 1993:485–88
56. Kepinski L, Okal J. 2000. Occurrence and mechanism of formation of CeOCl in Pd/CeO<sub>2</sub> catalysts. *J. Catal.* 192:48–53
57. Hungria AB, Martinez-Arias A, Fernandez-Garcia M, Iglesias-Juez A, Guerrero-Ruiz A, et al. 2003. Structural, morphological, and oxygen handling properties of nanosized cerium-terbium mixed oxides prepared by microemulsion. *Chem. Mater.* 15:4309–16
58. Martinez-Arias A, Fernandez-Garcia M, Iglesias-Juez A, Hungria AB, Anderson JA, et al. 2001. New Pd/Ce<sub>x</sub>Zr<sub>1-x</sub>O<sub>2</sub>/Al<sub>2</sub>O<sub>3</sub> three-way catalysts prepared by microemulsion: Part 2. In situ analysis of CO oxidation and NO reduction under stoichiometric CO+NO+O<sub>2</sub>. *Appl. Catal. B* 31:51–60
59. Hungria AB, Iglesias-Juez A, Martinez-Arias A, Fernandez-Garcia M, Anderson JA, et al. 2002. Effects of copper on the catalytic properties of bimetallic Pd-Cu/(Ce,Zr)O<sub>x</sub>/Al<sub>2</sub>O<sub>3</sub> and Pd-Cu/(Ce,Zr)O<sub>x</sub> catalysts for CO and NO elimination. *J. Catal.* 206:281–94
60. Martinez-Arias A, Fernandez-Garcia M, Salamanca LN, Valenzuela RX. 2000. Structural and redox properties of ceria in alumina-supported ceria catalyst supports. *J. Phys. Chem. B* 104:4038–46
61. Bera P, Patil KC, Jayaram V, Subbanna GN, Hegde MS. 2000. Ionic dispersion of Pt and Pd on CeO<sub>2</sub> by combustion method: effect of metal-ceria interaction on catalytic activities for NO reduction and CO and hydrocarbon oxidation. *J. Catal.* 196:293–301
62. Bera P, Gayen A, Hegde MS, Lalla NP, Spadaro L, et al. 2003. Promo effect of CeO<sub>2</sub> in combustion synthesis Pt/CeO<sub>2</sub> catalyst for CO oxidation. *J. Phys. Chem. B* 107:6122–30
63. Vlaic G, Fornasiero P, Martra G, Fonda E, Kaspar J, et al. 2000. Morphology of rhodium particles in ex-chloride Rh/Ce<sub>0.5</sub>Zr<sub>0.5</sub>O<sub>2</sub> catalyst. *J. Catal.* 190:182–90
64. Herz RK, Shlnouskls EJ. 1985. Application of high-resolution analytical electron microscopy to the analysis of automotive catalysts. *Ind. Eng. Chem. Prod. Res.* 24:6–10
65. Larese C, Galisteo FC, Granados ML, Mariscal R, Fierro JLG, et al. 2003. Deactivation of real three way catalysts by CePO<sub>4</sub> formation. *Appl. Catal. B* 40:305–17
66. Graham GW, O'Neill AE, Uy D, Weber WH, Sun H, Pan XQ. 2002. Observation of strained PdO in an aged Pd/ceria-zirconia catalyst. *Catal. Lett.* 79:99–105
67. Jiang JC, Pan XQ, Graham GW, McCabe RW, Shwank J. 2004. Microstructure of a Pd/ceria-zirconia catalyst after high-temperature aging. *Catal. Lett.* 53:37–42
68. Burch R. 1997. Low NO<sub>x</sub> options in catalytic combustion and emission control. *Catal. Today* 35:27
69. Graham GW, Jen HW, Chun W, McCabe RW. 1997. Encapsulation of Pd particles by ceria-zirconia mixed oxides. *Catal. Lett.* 44:185
70. Neyestanaki AK, Klingstedt F, Salmi T, Murzin DY. 2004. Deactivation of

- postcombustion catalysts, a review. *Fuel* 83:395–408
71. Skinjoh H, Muraki H, Fujitani Y. 1991. Effect of severe thermal aging on noble metal catalysts. In *Catalysis and Automotive Control II*, ed. A Cruq, p. 617. Amsterdam: Elsevier
72. Mabilon G, Durand D, Prigent M. 1991. Kinetics of the physico chemical and catalytic activity evolution of a platinum-rhodium catalyst in automotive exhaust gas. In *Catalysis and Automotive Control II*, ed. A Cruq, p. 569. Amsterdam: Elsevier
73. Bernal S, Calvino JJ, Cauqui MA, Gatica JM, Larese C, et al. 1999. Some recent results on metal/support interaction effects in NM/CeO<sub>2</sub> (NM: noble metal) catalysts. *Catal. Today* 50:175–206
74. Bernal S, Calvino JJ, Cauqui MA, Omil JAP, Pintado JM, Rodriguez-Izquierdo JM. 1998. Image simulation and experimental HREM study of the metal dispersion in Rh/Ce O<sub>2</sub> catalysts. Influence of the reduction/reoxidation conditions. *Appl. Catal. B* 16:127–38
75. Bernal S, Blanco G, Calvino JJ, Gatica JM, Omil JAP, Pintado JM. 2004. Characterisation of three-way automotive aftertreatment catalysts and related model systems. *Top. Catal.* 28:31–45
76. Bernal S, Cauqui MA, Cifredo GA, Gatica JM, Larese C, Omil JAP. 1996. Chemical and microstructural investigation of Pt/Ce O<sub>2</sub> catalysts reduced at temperatures ranging from 473 to 973 K. *Catal. Today* 29:77–81
77. Bernal S, Calvino JJ, Gatica JM, Lopez-Cartes C, Pintado JM. 2002. Chemical and nano-structural aspects of the preparation and characterisation of ceria and ceria-based mixed oxide-supported metal catalysts. In *Catalysis by Ceria and Related Materials*, ed. A Trovarelli, pp. 85–168. London: Imperial College Press
78. Gatica JM, Baker RT, Fornasiero P, Bernal S, Blanco G, Kaspar J. 2000. Rhodium dispersion in a Rh/Ce<sub>0.68</sub>Zr<sub>0.32</sub>O<sub>2</sub> catalyst investigated by HRTEM and H-2 chemisorption. *J. Phys. Chem. B* 104:4667–72
79. Gatica JM, Baker RT, Fornasiero P, Bernal S, Kaspar J. 2001. Characterization of the metal phase in NM/Ce<sub>0.68</sub>Zr<sub>0.32</sub>O<sub>2</sub> (NM: Pt and Pd) catalysts by hydrogen chemisorption and HRTEM microscopy: a comparative study. *J. Phys. Chem. B* 105:1191–99
80. Bernal S, Botana FJ, Calvino JJ, Cifredo GA, Perez Omil JA. 1995. HREM study of the behavior of a Rh/CeO<sub>2</sub> catalyst under high-temperature reducing and oxidizing conditions. *Catal. Today* 23:219–50
81. Bernal S, Blanco G, Calvino JJ, Lopez-Cartes C, Perez-Omil JA, et al. 2001. Electron microscopy (HREM, EELS) study of the reoxidation conditions for recovery of NM/CeO<sub>2</sub> (NM: Rh, Pt) catalysts from decoration or alloying phenomena. *Catal. Lett.* 76:131–37
82. Hickey N, Fornasiero P, Di Monte R, Kaspar J, Gonzalez-Velasco JR, et al. 2004. Reactivation of aged model Pd/Ce<sub>0.68</sub>-Zr<sub>0.32</sub>O<sub>2</sub> three-way catalyst by high temperature oxidising treatment. *Chem. Commun.* 196–97
83. Lassi U, Hietikko M, Rahkamaa-Tolonen K, Kallinen K, Savimäki A, et al. 2004. Deactivation correlations over Pd/Rh monoliths: the role of gas phase composition. *Top. Catal.* 30/31:457–61
84. Bernal S, Botana FJ, Calvino JJ, Lopez-Cartes C, Perez-Omil JA, Rodriguez-Izquierdo JM. 1998. The interpretation of HREM images of supported metal catalysts using image simulation: profile view images. *Ultramicroscopy* 72:135–64
85. Concepción P, Corma A, Silvestre-Alberto J, Franco V, Chane-Ching JY. 2004. Chemoselective hydrogenation catalysts: Pt on mesostructured CeO<sub>2</sub> nanoparticles embedded within ultrathin layers of SiO<sub>2</sub>. *J. Am. Chem. Soc.* 126: 5523–32
86. Bernal S, Blanco G, Calvino JJ, Lopez-Cartes C, Perez-Omil JA, et al. 2001.

- Electron microscopy (HREM, EELS) study of the reoxidation conditions for recovery of NM/CeO<sub>2</sub> (NM: Rh, Pt) catalysts from decoration or alloying phenomena. *Catal. Lett.* 76:131–37
87. Bernal S, Blanco G, Gatica JM, Larese C, Vidal H. 2001. Effect of mild re-oxidation treatments with CO<sub>2</sub> on the chemisorption capability of a Pt/CeO<sub>2</sub> catalyst reduced at 500 degrees C. *J. Catal.* 200:411–15
88. Deleted in proof
89. Bernal S, Botana FJ, Calvino JJ, Lopez-Cartes C, Perez-Omil JA, Rodriguez-Izquierdo JM. 1998. The interpretation of HREM images of supported metal catalysts using image simulation: profile view images. *Ultramicroscopy* 72:135–64
90. Rodriguez-Izquierdo JM, Bernal S, Cauqui MA, Finol D, Perez-Omil JA, et al. 1998. Characterization of La<sub>2</sub>O<sub>3</sub>/SiO<sub>2</sub> mixed oxide catalyst supports. *Am. Chem. Soc. Abstr.* 215:U484
91. Bernal S, Calvino JJ, Cauqui MA, Cifredo GA, Jobacho A, Rodriguez-Izquierdo JM. 1993. Metal-support interaction phenomena in rhodium ceria and rhodium titania catalysts—comparative study by high-resolution transmission electron spectroscopy. *Appl. Catal. A* 99:1–8
92. Bernal S, Calvino JJ, Cauqui MA, Gatica JM, Cartes CL, et al. 2003. Some contributions of electron microscopy to the characterisation of the strong metal-support interaction effect. *Catal. Today* 77:385–406
93. Baker RT, Calvino JJ, Lopez-Cartes C, Mira C, Perez-Omil JA, Rodriguez-Izquierdo JM. 1999. Detection and quantification of small misalignments in nanometer-sized particles on oxide support systems by the analysis of plan view HREM images. *Inst. Phys. Conf. Ser.* 161:537–40
94. Blanco G, Calvino JJ, Cauqui MA, Corchado P, Lopez-Cartes C, et al. 1999. Nanostructural evolution under reducing conditions of a Pt/CeTbOx catalyst: new alternative system as a TWC component. *Chem. Mater.* 11:3610–19
95. Bernal S, Calvino JJ, Gatica JM, Larese C, Lopez-Cartes C, Perez-Omil JA. 1997. Nanostructural evolution of a Pt/CeO<sub>2</sub> catalyst reduced at increasing temperatures (473–1223 k): a HREM study. *J. Catal.* 169:510–15
96. Penner S, Rupprechter G, Sauer H, Su DS, Tessadri R, et al. 2003. Pt/ceria thin film model catalysts after high-temperature reduction: a (HR)TEM study. *Vacuum* 71:71–76
97. Jenewein B, Fuchs M, Hayek K. 2003. The CO methanation on Rh/CeO<sub>2</sub> and CeO<sub>2</sub>/Rh model catalysts: a comparative study. *Surf. Sci.* 532–535:364–69
98. Penner S, Wang D, Su DS, Rupprechter G, Podlucky R, et al. 2003. Platinum nanocrystals supported by silica, alumina and ceria: metal-support interaction due to high-temperature reduction in hydrogen. *Surf. Sci.* 532–35:276–80
99. Kepinski L, Wolczyk M. 1997. Microstructure of Pd/CeO<sub>2</sub> catalyst: effect of high temperature reduction in hydrogen. *Appl. Catal. A* 150:197–220
100. Datye AK, Kalakkad D, Yao MH, Smith DJ. 1995. Comparison of metal-support interactions in Pt/TiO<sub>2</sub> and Pt/CeO<sub>2</sub>. *J. Catal.* 155:148–53
101. Datye AK, Kalakkad D, Robota HJ. 1994. Metal support interactions. *J. Catal.* 148:729–36
102. Kalakkad D, Datye A, Robota H. 1992. Interaction of Pt and ceria probed by transmission electron microscopy and catalytic reactivity. *Appl. Catal. B* 1:191–219
103. Cochrane HD, Hutchinson JL, White D, Parkinson GM, Dupas C, Scott AJ. 1990. High resolution electron microscopy of ceria-supported catalysts. *Ultramicroscopy* 34:10–16
104. Hayek K, Fuchs M, Klötzer B, Reichl W, Rupprechter G. 2000. Studies of metal-support interactions with “real” and “inverted” model systems: reactions of CO and small hydrocarbons with hydrogen on noble metals in contact with oxides. *Top. Catal.* 13:55–66

105. Bitter H, Cauqui MA, Gatica JM, Bernal S, Ramaker DE, Koningsberger DC. 2000. Changes in the electronic structure of Pt/CeO<sub>2</sub> based DeNO<sub>x</sub> catalysts as a function of the reduction treatment. Detection of a Pt-H anti-bonding shape resonance and Pt-H EXAFS. *Stud. Surf. Sci. Catal.* 130D:3183–88
106. Bernal S, Botana FJ, Calvino JJ, Lopez C, Perez-Omil JA, Rodriguez-Izquierdo JM. 1996. High-resolution electron microscopy investigation of metal-support interactions in Rh/TiO<sub>2</sub>. *J. Chem. Soc. Faraday Trans.* 92:2799–809
107. Hayek K, Bernd J, Klotzer B, Reichl W. 2001. Surface reactions on inverse model catalysts: CO adsorption and CO hydrogenation on vanadia- and ceria-modified surfaces of rhodium and palladium. *Top. Catal.* 14:25–33
108. Wang D, Penner S, Su DS, Rupprechter G, Hayek K, Schlögl R. 2003. Silicide formation on a Pt/SiO<sub>2</sub> model catalyst studied by TEM, EELS, and EDXS. *J. Catal.* 219:434–41
109. Gai PL, Boyes ED. 1997. Environmental HREM in materials science. In *In situ Microscopy in Materials Research*, ed. PL Gai, pp. 123–40. Dordrecht: Kluwer
110. Sharma R, Weiss K. 1998. Development of a TEM to study in situ structural and chemical changes during gas-solid interactions at elevated temperature. *Microsc. Res. Tech.* 42:270–80
111. Lopez-Cartes C, Bernal S, Calvino JJ, Cauqui MA, Blanco G, et al. 2003. In situ transmission electron microscopy investigation of Ce(IV) and Pr(IV) reducibility in a Rh (1%)/Ce<sub>0.8</sub>Pr<sub>0.2</sub>O<sub>2-x</sub> catalyst. *Chem. Commun.* 644–45
112. Bernal S, Calvino JJ, Cauqui MA, Lopez-Cartes C, Perez-Omil JA. 2001. The role of metal-support interaction on the oxidation of noble metals supported on cerium based oxides. *Inst. Phys. Conf. Ser.* 168:389–92
113. Rocchini E, Vicario M, Llorca J, de Leitenburg C, Dolcetti G, Trovarelli A. 2002. Reduction and oxygen storage behavior of noble metals supported on silica-doped ceria. *J. Catal.* 211:407–21
114. Bernal S, Calvino JJ, Cifredo GA, Finol D, Gatica JM, et al. 2002. Study of the structural modifications induced by reducing treatments on a Pd/Ce<sub>0.8</sub>Tb<sub>0.2</sub>O<sub>2-x</sub>/La<sub>2</sub>O<sub>3</sub>-Al<sub>2</sub>O<sub>3</sub> catalyst by means of X-ray diffraction and electron microscopy techniques. *Chem. Mater.* 14:1405–10
115. Kepinski L, Wolczyk M, Marchewka M. 2002. Structure evolution of nanocrystalline CeO<sub>2</sub> supported on silica: effect of temperature and atmosphere. *J. Solid State Chem.* 168:110–18
116. Kang ZC, Eyring L. 2000. Lattice oxygen transfer in fluorite-type oxides containing Ce, Pr, and/or Tb. *J. Solid State Chem.* 155:129–37
117. Sasaki T, Ukyo Y, Suda A, Sugiura M, Kuroda K, et al. 2003. Oxygen absorption behavior of Ce<sub>2</sub>Zr<sub>2</sub>O<sub>7+x</sub> and formation of Ce<sub>2</sub>Zr<sub>2</sub>O<sub>7.5</sub>. *J. Ceram. Soc. Jpn.* 111:382–85
118. Baker RT, Bernal S, Lopez-Cartes C, Perez-Omil JA, Montardi Y. 1999. Investigation of redox-cycled Ce-Zr mixed oxides for automotive catalysts by electron microscopy. *Electron Microsc. Anal.* 3: 521–24
119. Masui T, Ozaki T, Adachi G, Kang ZC, Eyring L. 2000. A new ceria-zirconia mixed oxide phase based on pyrochlore. *Chem. Lett.* 7:240–41
120. Rupprechter G, Hayek K, Hofmeister H. 1998. Electron microscopy of thin-film model catalysts: activation of alumina-supported rhodium nanoparticles. *J. Catal.* 173:409–22
121. Cunningham J, Cullinane D, Farrell F, Morris MA, Datye AK, Kalakkad D. 1995. Changes in microstructure and catalytic activity effected by redox cycling of rhodium upon CeO<sub>2</sub> and Al<sub>2</sub>O<sub>3</sub>. *Stud. Surf. Sci. Catal.* 96:237–48
122. Deleted in proof
123. Bernal S, Blanco G, Cauqui MA, Corchado P, Pintado JM, Rodriguez Izquierdo

- JM. 1997. Oxygen buffering capacity of mixed cerium terbium oxide: a new material with potential applications in three-way catalysts. *Chem. Commun.* 1545–46
124. Lyubovsky M, Pfefferle L, Datye A, Bravo J, Nelson T. 1999. TEM study of the microstructural modifications of an alumina-supported palladium combustion catalyst. *J. Catal.* 187:275–84
125. Datye AK, Bravo J, Nelson T, Atanasova P, Lyubovsky M, Pfefferle L. 2000. Catalyst microstructure and methane oxidation reactivity during the Pd-PdO transformation on alumina supports. *Appl. Catal. A* 198:179–96
126. Sharma R, Crozier PA. 1999. In situ electron microscopy of CeO<sub>2</sub> and CeO<sub>2</sub>-ZrO<sub>2</sub> reduction. *Inst. Phys. Conf. Ser.* 161:569–72
127. Sharma R, Crozier PA, Kang ZC, Eyring L. 2004. Observation of dynamic nanostructural and nanochemical changes in ceria-based catalysts during in-situ reduction. *Philos. Mag.* 84:2731–47
128. Baker RT, Bernal S, Blanco G, Gatica JM, Pintado JM, et al. 1999. Reversible changes in the redox behaviour of Ce<sub>0.68</sub>-Zr<sub>0.320</sub> mixed oxide: effect of alternating the re-oxidation temperature after reduction at 1223 K. *Chem. Commun.* 149–50
129. Izu N, Kishimoto HOT, Ono K, Ozuka-Yao-Matsuo S. 2001. *Adv. Mater.* 2:397–440
130. Allard LF, Völkl A, Carim A, Datye AK, Rouff R. 1996. Morphology and crystallography of nanoparticulates revealed by electron holography. *Nanostruct. Mater.* 7:137–46
131. Shelef M. 1995. Selective catalytic reduction of NO<sub>x</sub> with N-free reductants. *Chem. Rev.* 95:209–25
132. Coudurier G, Vedrine JC. 2000. EURO-CAT oxide: a European V<sub>2</sub>O<sub>5</sub>-WO<sub>3</sub>/TiO<sub>2</sub> SCR standard catalyst study: characterisation by electron microscopies (SEM, HRTEM, EDX) and by atomic force microscopy. *Catal. Today* 56:415–30
133. Lisi L, Lasorella G, Malloggi S, Russo G. 2004. Single and combined deactivating effect of alkali metals and HCl on commercial SCR catalysts. *Appl. Catal. B* 50:251–58
134. Reddy EP, Rojas TC, Fernández A. 2000. Transmission electron microscopy and energy-dispersive X-ray spectroscopy study of V<sub>2</sub>O<sub>5</sub>/TiO<sub>2</sub>-ZrO<sub>2</sub>. *Langmuir* 16:4217–21
135. Herman RG, Sale JW, Harvey G, Stenger J, Lyman CE, et al. 2002. Monitoring aging and deactivation of emission abatement catalysts for selective catalytic reduction of NO<sub>x</sub>. *Top. Catal.* 18:251–57
136. Hoang-Van C, Zeogaoui O, Pichat P. 1998. Vanadian-titania aerogel deNO<sub>x</sub> catalysts. *J. Non-Cryst. Solids* 225:157–62
137. Bogdanchikova N, Meunier FC, Avalos-Borja M, Breen JP, Pestryakov A. 2002. On the nature of the silver phases of Ag/Al<sub>2</sub>O<sub>3</sub> catalysts for reactions involving nitric oxide. *Appl. Catal. B* 36:287–97
138. Hickey N, Fornasiero P, Kaspar J, Graziani M, Martra G, et al. 2002. Improvement of SO<sub>x</sub>-resistance of silver lean-DeNO<sub>x</sub> catalysts by supporting on CeO<sub>2</sub>-containing zirconia. *J. Catal.* 209:271–74
139. Richter M, Langpape M, Kolf S, Grubert G, Eckelt R, et al. 2002. Combinatorial preparation and high-throughput catalytic tests of multi-component deNO<sub>x</sub> catalysts. *Appl. Catal. B* 36:261–77
140. Fuentes S, Bogdanchikova N, Avalos-Borja M, Boronin A, Farias MH, et al. 2000. Structural and catalytic properties of Pd/Al<sub>2</sub>O<sub>3</sub>-La<sub>2</sub>O<sub>3</sub> catalysts. *Catal. Today* 55:301–9
141. Macleod N, Cropley R, Keel JM, Lambert RM. 2004. Exploiting the synergy of titania and alumina in lean NO<sub>x</sub> reduction: in situ ammonia generation during the Pd/TiO<sub>2</sub>/Al<sub>2</sub>O<sub>3</sub>-catalysed H<sub>2</sub>/CO/NO/O<sub>2</sub> reaction. *J. Catal.* 221:20–31
142. Sun K, Liu J, Browning ND. 2002. Direct atomic scale analysis of the distribution

- of Cu valence states in Cu/ $\gamma$ -Al<sub>2</sub>O<sub>3</sub> catalysts. *Appl. Catal. B* 38:271–81
143. Balint I, Miyazaki A. 2004. NO/CH<sub>4</sub> reaction over nanodispersed Pt particles. *Top. Catal.* 30/31:123–26
144. Okal J, Kepinski L, Krajczyk L, Tylus W. 2003. Oxidation and redispersion of a low-loaded Re/ $\gamma$ -Al<sub>2</sub>O<sub>3</sub> catalyst. *J. Catal.* 219:362–71
145. Okal J, Kepinski L, Krajczyk L, Drozd M. 1999. Oxidation and redispersion of a Re/ $\gamma$ -Al<sub>2</sub>O<sub>3</sub> catalyst. *J. Catal.* 188:140–45
146. Serre C, Auroux A, Gervasini A, Hervieu M, Férey G. 2002. Hexagonal and cubic thermally stable mesoporous tin(IV) phosphates with acidic and catalytic properties. *Angew Chem. Int. Ed.* 41:1594–97
147. Perez-Ramirez J, Garcia-Cortes JM, Kapteijn F, Mul G, Moulijn JA, et al. 2001. Characterization and performance of Pt-USY in the SCR of NO<sub>x</sub> with hydrocarbons under lean-burn conditions. *Appl. Catal. B* 29:285–98
148. Garcia-Cortes JM, Perez-Ramirez J, Rouzaud JN, Vaccaro AR, Illan-Gomez MJ, et al. 2003. On the structure sensitivity of deNO<sub>x</sub> HC-SCR over Pt-beta catalysts. *J. Catal.* 218:111–22
149. Wögerbauer C, Maciejewski M, Baiker A, Göbel U. 2001. Ir/H-ZSM-5 catalysts in the selective reduction of NO<sub>x</sub> with hydrocarbons. *Top. Catal.* 16/17:181–86
150. Gai PL. 1983. In situ ETEM of redox studies of V<sub>2</sub>O<sub>5</sub> catalysts. *Philos. Mag.* 48: 359–65
151. Kryukova GN, Zenkovets GA, Pfander N, Su D-S, Schlogl R. 2003. Synthesis and characterization of the titanium doped nanostructural V<sub>2</sub>O<sub>5</sub>. *Mater. Sci. Eng. A* 343:8–12
152. Su DS, Zandbergen HW, Tiemeijer PC, Kothleitner G, Hävecker M, et al. 2003. High resolution EELS using monochromator and high performance spectrometer: comparison of <V<sub>2</sub>O<sub>5</sub> ELNES with NEXAFS and band structure calculations. *Micron* 34:235–38
153. Su DS, Hébert C, Willinger M, Schlogl R. 2003. Anisotropy and collection angle dependence of the oxygen K ELNES in V<sub>2</sub>O<sub>5</sub>: a band-structure calculation study. *Micron* 34:227–33
154. Hébert C, Willinger M, Pongratz P, Shattschneider P, Schlogl R. 2002. Oxygen K-edge in vanadium oxides: simulations and experiments. *Eur. Phys. J.* 28:407–14
155. Baudin F, Da Costa P, Thomas C, Calvo S, Lendresse Y, et al. 2004. No<sub>x</sub> reduction over CeO<sub>2</sub>-ZrO<sub>2</sub> supported iridium catalyst in the presence of propanol. *Top. Catal.* 30/31:97–101
156. Ziese U, de Jong KP, Koster AJ. 2004. Electron tomography: a tool for 3D structural probing of heterogeneous catalysts at the nanometer scale. *Appl. Catal. A* 260:71
157. Koster AJ, Ziese U, Verkleij AJ, Janssen AH, Jong KP. 2000. Three-dimensional transmission electron microscopy: a novel imaging and characterization technique with nanometer scale resolution for materials science. *J. Phys. Chem. B* 104:9368–70
158. Janssen AH, Koster AJ, Jong KP. 2002. On the shape of the mesopores in zeolite Y: a three-dimensional transmission electron microscopy study combined with texture analysis. *J. Phys. Chem. B* 106:11905–9
159. Janssen AH, Yang CM, Wang Y, Schüth F, Koster AJ, Jong KP. 2003. Localization of small metal (oxide) particles in SBA-15 using bright-field electron tomography. *J. Phys. Chem. B* 107:10552–56
160. Weyland M, Midgley PA. 2001. High spatial resolution tomographic reconstruction from STEM high angle annular dark field (HAADF) images. *Inst. Phys. Conf. Ser.* 168:107
161. Midgley PA, Weyland M, Thomas JM, Johnson FG. 2001. Z-contrast tomography: a technique in three-dimensional nanostructural analysis based on Rutherford scattering. *Chem. Commun.* 907–8

162. Weyland M. 2002. Electron tomography of catalyst. *Top. Catal.* 21:175–83
163. Gai PL, Kourtakis K, Ziemiecki S. 2000. In situ real-time environmental-TEM of nanometer size xerogel catalysts. *Microw. Microanal.* 6:335–42
164. Avci AK, Ilse OZ, Trimm DL. 2001. On-board fuel conversion for hydrogen fuel cells: comparison of different fuels by computer simulations. *Appl. Catal. A* 216(1–2):243
165. Carrette L, Friedrich KA, Stimming U. 2000. Fuel cells: principles, types, fuels, and applications. *Chem. Phys. Chem.* 1:162
166. Tomishige K, Asadullah M, Kunimori K. 2004. Syngas production by biomass gasification using Rh/CeO<sub>2</sub>/SiO<sub>2</sub> catalysts and fluidized bed reactor. *Catal. Today* 89:389–403
167. Asadullah M, Ito S, Kunimori K, Yamada M, Tomishige K. 2002. Biomass gasification to hydrogen and syngas at low temperature: novel catalytic system using fluidized-bed reactor. *J. Catal.* 208:255–59
168. Kiros Y, Schwartz S. 2000. Long-term hydrogen oxidation catalysts in alkaline fuel cells. *J. Power Sources* 87:101–5
169. Löffler MS, Grob B, Natter H, Hempelmann R, Krrajewski T, Divisek J. 2001. Synthesis and characterization of catalyst layers for direct methanol fuel cell applications. *Phys. Chem. Chem. Phys.* 3:333–36
170. Zhang YJ, Maroto-Valiente A, Rodriguez-Ramos I, Xin Q, Guerrero-Ruiz A. 2004. Synthesis and characterization of carbon black supported Pt-Ru alloy as a model catalyst for fuel cells. *Catal. Today* 93–95:619–26
171. Li W, Zhou W, Li H, Zhou Z, Zhou B, et al. 2004. Nano-structured Pt-Fe/C as cathode catalyst in direct methanol fuel cell. *Electrochim. Acta* 49:1045–55
172. Staiti P, Arico AS, Antonucci V, Hocevar S. 1998. Morphological variation of platinum catalysts in phosphotungstic acid fuel cell. *J. Power Sources* 70:91–101
173. Aupretre F, Descorme C, Duprez D. 2004. Hydrogen production for fuel cells from the catalytic ethanol steam reforming. *Top. Catal.* 30/31:487–91
174. Llorca J, Homs N, Sales J, de la Piscina PR. 2002. Efficient production of hydrogen over supported cobalt catalysts from ethanol steam reforming. *J. Catal.* 209:306–17
175. Verykios XE. 2003. Catalytic dry reforming of natural gas for the production of chemicals and hydrogen. *Int. J. Hydrogen Energy* 28:1045–63
176. Liguras DK, Goundani K, Verykios XE. 2004. Production of hydrogen for fuel cells by catalytic partial oxidation of ethanol over structured Ni catalysts. *J. Power Sources* 130:30–37
177. Kang ZC, Eyring L. 2001. Hydrogen production from methane and water by lattice oxygen transfer with Ce<sub>0.70</sub>-Zr<sub>0.25</sub>Tb<sub>0.05</sub>O<sub>2-x</sub>. *J. Alloys Compounds* 323–324:97–101
178. Masui T, Nakano K, Ozaki T, Adachi G, Kang ZC, Eyring L. 2001. Redox behavior of ceria-zirconia solid solution modified by the chemical filing process. *Chem. Mater.* 13:1834–40
179. Kang ZC, Wang ZL. 2003. Novel oxides for cycled hydrogen production from methane and water using a temperature swing. *Adv. Mater.* 15:521–26
180. Basinska A, Kepinski L, Domka F. 1999. The effect of support on WGS activity of ruthenium catalysts. *Appl. Catal. A* 183:143–53
181. Hartmann M, Bischof C, Luan Z, Kevin L. 2001. Preparation and characterization of ruthenium clusters on mesoporous support. *Microporous Mesoporous Mater.* 44–45:385–94
182. Fu Q, Weber A, Flytzany-Stephanopoulos M. 2001. Nanostructured Au-CeO<sub>2</sub> catalysts for low-temperature water-gas shift. *Catal. Lett.* 77:87–95
183. Panzera G, Modafferi V, Candamano S,

- Donato A, Frusteri F, Antonucci PL. 2004. CO selective oxidation on ceria-supported Au catalysts for fuel cell application. *J. Power Sources* 135:177–83
184. Bulushev DA, Kiwi-Minsker L, Yuranov I, Suvorova EI, Buffat PA, Renken A. 2002. Structured Au/FeO<sub>x</sub>/C catalysts for low-temperature CO oxidation. *J. Catal.* 210:149–59
185. Choudhary TV, Sivadinarayana C, Chusuei CC, Datye AK, Fackler J, Goodman DW. 2002. CO oxidation on supported nano-Au catalysts synthesized from a [Au<sub>6</sub>(PPh<sub>3</sub>)<sub>6</sub>](BF<sub>4</sub>)<sub>2</sub> complex. *J. Catal.* 207:247–55
186. Bera P, Hegde MS. 2004. Characterization and catalytic properties of combustion synthesized Au/CeO<sub>2</sub> catalyst. *Catal. Lett.* 79:75–81
187. Lopez N, Norskov JK, Janssens TVW, Carlsson A, Puig-Molina A, et al. 2004. The adhesion and shape of nanosized Au particles in a Au/TiO<sub>2</sub> catalyst. *J. Catal.* 225:86–94
188. Liu X, Korotkikh O, Farrauto R. 2002. Selective catalytic oxidation of CO in H<sub>2</sub>: structural study of Fe oxide-promoted Pt/alumina catalyst. *Appl. Catal. A* 226:293–303
189. Akita T, Ichikawa S, Tanaka K, Haruta M. 2001. Analytical TEM study on the dispersion of Au nanoparticles in Au/TiO<sub>2</sub> catalyst prepared under various temperatures. *Surf. Interface Anal.* 31:73–78
190. Chen YJ, Yeh CT. 2001. Deposition of highly dispersed gold on alumina support. *J. Catal.* 200:59–68
191. Deluga GA, Salge JR, Verykios XE. 2004. Renewable hydrogen from ethanol by autothermal reforming. *Science* 303:993–97
192. Eyring L, Kang ZC. 2000. *Patent No. WO2000025898*
193. Fatsikostas AN, Verykios XE. 2004. Reaction network of steam reforming of ethanol over Ni-based catalysts. *J. Catal.* 225:439–52
194. Luo JZ, Yu ZL, Ng CF, Au CT. 2000. CO<sub>2</sub>/CH<sub>4</sub> reforming over Ni-La<sub>2</sub>O<sub>3</sub>/5A: an investigation on carbon deposition and reaction steps. *J. Catal.* 194:198–210
195. Bernal S, Botana FJ, Calvino JJ, Cifredo GA, Garcia R, Rodriguez-Izquierdo JM. 1990. HREM characterization of metal-catalysts supported on rare-earth-oxides—samarium oxide as support. *Ultra-microscopy* 34:60–65
196. Bernal S, Calvino JJ, Lopez-Cartes C, Pintado JM, Perez-Omil JA, et al. 1999. Nanostructural evolution of high loading Rh/lanthana catalysts through the preparation and reduction steps. *Catal. Today* 52:29–43
197. Bernal S, Calvino JJ, Cauqui MA, Gatica JM, Cartes CL, et al. 2003. Some contributions of electron microscopy to the characterisation of the strong metal-support interaction effect. *Catal. Today* 77:385–406
198. Haruta M, Tsubota S, Kobayashi T, Kageyama H, Genet M, Delmon B. 1993. Low-temperature oxidation of CO over gold supported on TiO<sub>2</sub>, Fe<sub>2</sub>O<sub>3</sub>, and Co<sub>3</sub>O<sub>4</sub>. *J. Catal.* 144:175–79
199. Haruta M. 1997. Size- and support-dependency in the catalysis of gold. *Catal. Today* 36:153–66
200. Ichikawa S, Akita T, Okumura M, Kohyama M, Tanaka K. 2003. Electron holographic analysis of nanostructured gold catalyst. *JEOL News* 38:6–9
201. Ichikawa S, Akita T, Okumura M, Haruta M, Tanaka K, Kohyama M. 2003. Electron holographic 3D nanoanalysis of Au/TiO<sub>2</sub> catalyst at interface. *J. Electron Microsc.* 52:21–26
202. Akita T, Tanaka K, Tsubota S, Haruta M. 2000. Analytical high resolution TEM study of supported gold catalysts: orientation relationship between Au particles and TiO<sub>2</sub> supports. *J. Electron Microsc.* 49:657–62
203. Ichikawa S, Akita T, Okumura M, Haruta

- M, Tanaka K. 2002. Electron holographic nano-characterization of gold catalyst at interface. *Mater. Res. Soc. Symp. Proc.* 727:11–16
204. Centeno MA, Paulis M, Montes M, Odriozola JA. 2002. Catalytic combustion of volatile organic compounds on Au/CeO<sub>2</sub>/Al<sub>2</sub>O<sub>3</sub> and Au/Al<sub>2</sub>O<sub>3</sub> catalysts. *Appl. Catal. A* 234:65–78
205. Besson M, Kallel A, Gallezot P, Zanella R, Louis C. 2003. Gold catalysts supported on titanium oxide for catalytic wet air oxidation of succinic acid. *Catal. Commun.* 4:471–76

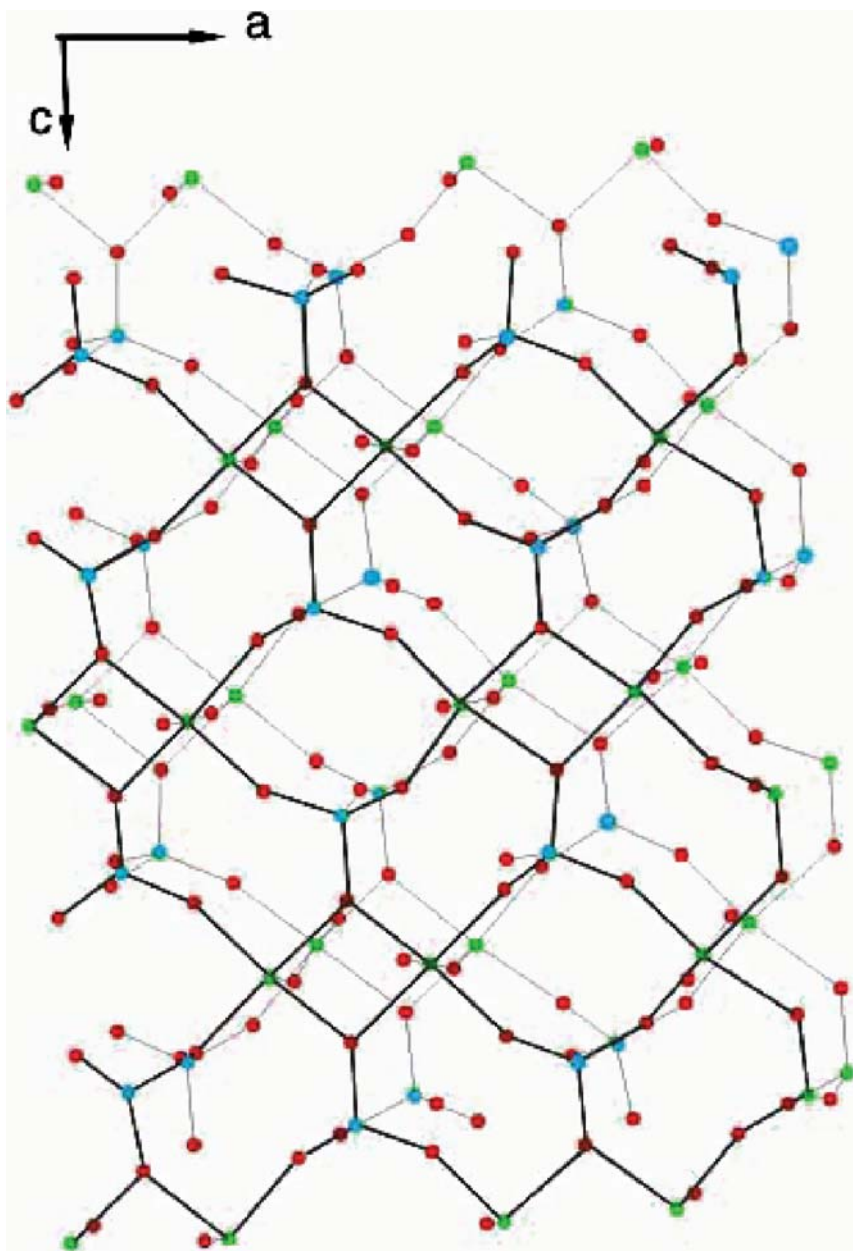


**Figure 2** (a) A three-dimensional structural model of VPO catalyst along [010] with edge-shared vanadyl octahedra interconnected by phosphate tetrahedra.



## CONTENTS

---

### MATERIALS DESIGN AND CHEMISTRY OF ENVIRONMENTALLY ACCEPTABLE CATALYSTS

- THE PREPARATION AND CHARACTERIZATION OF HIGHLY EFFICIENT  
TITANIUM OXIDE–BASED PHOTOFUNCTIONAL MATERIALS,  
*Masakazu Anpo, Satoru Dohshi, Masaaki Kitano, Yun Hu,  
Masato Takeuchi, and Masaya Matsuoka* 1
- APPLICATION OF EXAFS TO MOLTEN SALTS AND IONIC LIQUID  
TECHNOLOGY, *Christopher Hardacre* 29
- THE PREPARATION OF SKELETAL CATALYSTS, *A.J. Smith and D.L. Trimm* 127
- HETEROGENEOUS ASYMMETRIC CATALYSTS: STRATEGIES FOR ACHIEVING  
HIGH ENANTIOSELECTION, *Graham J. Hutchings* 143
- ENGINEERED POROUS CATALYTIC MATERIALS, *Ferdi Schüth* 209
- DESIGNING CATALYSTS FOR CLEAN TECHNOLOGY, GREEN CHEMISTRY,  
AND SUSTAINABLE DEVELOPMENT, *John Meurig Thomas  
and Robert Raja* 315
- POROUS ALUMINOPHOSPHATES: FROM MOLECULAR SIEVES TO DESIGNED  
ACID CATALYSTS, *H.O. Pastore, S. Coluccia, and L. Marchese* 351
- CHEMICAL DESIGN AND IN SITU CHARACTERIZATION OF ACTIVE  
SURFACES FOR SELECTIVE CATALYSIS, *Mizuki Tada  
and Yasuhiro Iwasawa* 397
- METAL CATALYST DESIGN AND PREPARATION IN CONTROL OF  
DEACTIVATION, *Michael S. Spencer and Martyn V. Twigg* 427
- ELECTRON MICROSCOPY IN THE CATALYSIS OF ALKANE OXIDATION,  
ENVIRONMENTAL CONTROL, AND ALTERNATIVE ENERGY SOURCES,  
*Pratibha L. Gai and Jose J. Calvino* 465

### CURRENT INTEREST

- THE DIFFUSION-MULTIPLE APPROACH TO DESIGNING ALLOYS,  
*Ji-Cheng (J.-C.) Zhao* 51
- SPATIAL ORDER AND DIFFRACTION IN QUASICRYSTALS AND BEYOND,  
*Denis Gratias, Lionel Bresson, and Marianne Quiquandon* 75

INFLUENCE OF INTERFACE ANISOTROPY ON GRAIN GROWTH AND COARSENING, <i>Gregory S. Rohrer</i>	99
THE OXIDATION OF NiAl: WHAT CAN WE LEARN FROM AB INITIO CALCULATIONS? <i>M.W. Finnis, A.Y. Lozovoi, and A. Alavi</i>	167
ANALYTICAL TRANSMISSION ELECTRON MICROSCOPY, <i>Wilfried Sigle</i>	239
COMPOSITE MATERIALS FOR WIND POWER TURBINE BLADES, <i>Povl Brøndsted, Hans Lilholt, and Aage Lystrup</i>	505
MATERIALS CHARACTERIZATION IN THE ABERRATION-CORRECTED SCANNING TRANSMISSION ELECTRON MICROSCOPE, <i>M. Varela, A.R. Lupini, K. van Benthem, A.Y. Borisevich, M.F. Chisholm, N. Shibata, E. Abe, and S.J. Pennycook</i>	539
ADHESION AND DE-ADHESION MECHANISMS AT POLYMER/METAL INTERFACES: MECHANISTIC UNDERSTANDING BASED ON IN SITU STUDIES OF BURIED INTERFACES, <i>G. Grundmeier and M. Stratmann</i>	571

**INDEXES**

Subject Index	617
Cumulative Index of Contributing Authors, Volumes 31–35	655
Cumulative Index of Chapter Titles, Volumes 31–35	657

**ERRATA**

An online log of corrections to *Annual Review of Materials Research* chapters may be found at <http://matsci.annualreviews.org/errata.shtml>